Analysis of induced seismicity in geothermal reservoirs – An overview

Arno Zang[a,*], Volker Oye[b], Philippe Jousset[c], Nicholas Deichmann[d], Roland Gritto[e],
Art McGarr[f], Ernest Majer[g], David Bruhn[c]

[a] *German Research Center for Geosciences (GFZ), Section 2.6 Seismic Hazard and Stress Field, Telegrafenberg, 14473 Potsdam, Germany*
[b] *NORSAR, P.O. Box 53, N-2027 Kjeller, Norway*
[c] *GFZ, International Center for Geothermal Research, 14473 Potsdam, Germany*
[d] *Swiss Seismological Service, ETH Zürich, Sonneggstrasse 5, CH-8092 Zürich, Switzerland*
[e] *Array Information Technology, 2020 Cedar Street, Berkeley, CA 94709, USA*
[f] *U.S. Geological Survey, Menlo Park, CA 94025, USA*
[g] *Lawrence Berkeley National Laboratory, Berkeley, CA 94720, USA*

ARTICLE INFO

ABSTRACT

In this overview we report results of analysing induced seismicity in geothermal reservoirs in various tectonic settings within the framework of the European Geothermal Engineering Integrating Mitigation of Induced Seismicity in Reservoirs (GEISER) project. In the reconnaissance phase of a field, the subsurface fault mapping, in situ stress and the seismic network are of primary interest in order to help assess the geothermal resource. The hypocentres of the observed seismic events (seismic cloud) are dependent on the design of the installed network, the used velocity model and the applied location technique. During the stimulation phase, the attention is turned to reservoir hydraulics (e.g., fluid pressure, injection volume) and its relation to larger magnitude seismic events, their source characteristics and occurrence in space and time. A change in isotropic components of the full waveform moment tensor is observed for events close to the injection well (tensile character) as compared to events further away from the injection well (shear character). Tensile events coincide with high Gutenberg-Richter b-values and low Brune stress drop values. The stress regime in the reservoir controls the direction of the fracture growth at depth, as indicated by the extent of the seismic cloud detected. Stress magnitudes are important in multiple stimulation of wells, where little or no seismicity is observed until the previous maximum stress level is exceeded (Kaiser Effect). Prior to drilling, obtaining a 3D P-wave (Vp) and S-wave velocity (Vs) model down to reservoir depth is recommended. In the stimulation phase, we recommend to monitor and to locate seismicity with high precision (decametre) in real-time and to perform local 4D tomography for velocity ratio (Vp/Vs). During exploitation, one should use observed and model induced seismicity to forward estimate seismic hazard so that field operators are in a position to adjust well hydraulics (rate and volume of the fluid injected) when induced events start to occur far away from the boundary of the seismic cloud.

1. Introduction

Over geological time scales tectonic forces build up stress in the Earth's crust (*Zang and Stephansson*, 2010). Apart from crustal creep, earthquakes are the primary brittle processes that partially relax stresses in the crust. Earthquakes of tectonic or volcanic origin occur when stresses on pre-existing planes of weakness exceed their strength (e.g., *Scholz*, 1990). Induced earthquakes are similar, but occur when either stress or strength are perturbed by natural or anthropogenic influences (e.g., *Trifu*, 2002). Naturally induced earthquakes have been associated with heavy rainfalls (e.g., *Grünthal*, 2014, induced seismicity category 7) or with transient surface waves from major tectonic earthquakes (e.g., *Jousset and Rohmer*, 2012). Man-made induced seismicity has been observed in numerous settings (e.g., *Trifu*, 2010). Among them are impoundment of lakes behind dams giving rise to reservoir-triggered seismicity (e.g., *Talwani and Acree*, 1985), mining-induced seismicity (e.g., *Mendecki*, 1997), the injection and

production at hydrocarbon reservoirs (e.g., *Suckale*, 2009) and the disposal of wastewater in the subsurface (e.g., *Healy et al.*, 1968). Induced seismicity related to deep geothermal applications has been studied for many years, e.g. as part of the Fenton Hill, New Mexico hot dry rock experiment (HDR, *Pearson*, 1981; *Bame and Fehler*, 1986; *Ferrazzini et al.*, 1990), but progress to understand this phenomenon slowed down soon after. Recently, induced seismicity in geothermal applications (geothermal seismicity) has attracted public interest due to issues of seismic risk (e.g., *Giardini*, 2009).

The goal in engineered or enhanced geothermal reservoir operations is to locate or safely create permeability through e.g. fractures in high-temperature rock such that water and steam can circulate through these pathways to efficiently transfer heat to the surface. While in the initial HDR concept, inclined injection and production wells are connected via discrete, parallel hydraulic tensile fractures (engineered geothermal system), in enhanced geothermal systems (EGS) the natural rock joint network permeability is increased by massive water injection in extended open-hole sections (*Jung*, 2013). *Tester et al.* (2006) defined EGS as engineered reservoirs designed to economically extract heat from low permeability formations. In places where fractures are not naturally occurring, new ones need to be created or existing ones reac-

* Corresponding author. Tel.: +49 331 288 1325; fax: +49 331 288 1127.
E-mail address: zang@gfz-potsdam.de (A. Zang).

tivated. Most EGS projects require drilling of boreholes to reach adequate temperatures at depth and pumping of fluids at high pressures to enhance permeability through hydraulic fracturing (mode I crack), hydro-shear (mode II crack), combination of both (mixed modes), or acidizing. In this article, geothermal seismicity (sensu stricto) is associated with the development and operation of EGS systems.

Hydraulic fracturing has become a standard technology in geothermal stimulation (*Bromley*, 2010) and has been for decades in oil and gas applications (*Maxwell et al.*, 2010). One of the challenges in EGS is to increase permeability in a way that the heat transfer is optimally efficient, which is a fundamental difference to the challenges in unconventional reservoirs (enhanced recovery). Pumping too much water, or too fast, or in a critically stressed fault may create excessive permeability, which may decrease the efficiency of the heat exchanger and also may induce larger magnitude events thereby increasing seismic hazard.

Induced seismicity in geothermal settings has been documented in areas such as Indonesia (*Silitonga et al.*, 2005; *Mulyadi*, 2010), the Philippines (*Bromley et al.*, 1986), Japan (*Nagano et al.*, 1994), Kenya (*Simiyu*, 1999), North and South America (*Henderson et al.*, 2002; *Yamabe and Hamza*, 1996), Australia (*Baisch et al.*, 2006) and New Zealand (*Hunt and Latter*, 1982) for over 40 years. In Europe, an early description of industrial exploitation of geothermal resources was published by *Batchelor and Garnish* (1990). Recently, *Evans et al.* (2012) compiled a survey of induced seismicity responses to fluid injection in European geothermal and CO_2 reservoirs.

Annually, thousands of seismic events are generated during exploitation of geothermal fields but in most cases these events are below local magnitude $M_L = 2$, and below the detection threshold of communities (e.g., *Evans et al.*, 2012). Geothermal sites in the Rhine Graben near Basel (*Deichmann and Giardini*, 2009), Landau (*Grünthal*, 2014) and Soultz-sous-Forêts (*Dorbath et al.*, 2009), however, have experienced $M_L > 2.5$ events due to EGS activities (Table 1). Although this seismicity has been short lived it has attracted public concern due to its proximity to populated areas (*Kraft et al.*, 2009). At other sites, geothermal seismicity is entirely of low magnitudes and then may drop below the detection threshold, possibly due to geologic conditions, e.g. high attenuation of seismic waves caused by overlying sediment formations. One example of low magnitude seismicity is the German site Groß Schönebeck. Even massive hydraulic stimulations performed by injection of 13,000 m^3 of water into the well Gt GrSk 4/05 produced only 80 seismic events with moment magnitudes in the range of −1.8 to −1.0 (*Kwiatek et al.*, 2010). Another example of low seismicity rate is the Bouillante geothermal field (French West Indies), where no earthquakes could be related to the exploitation of the geothermal field (*Sanjuan et al.*, 2010). A possible explanation could be the absence of reinjection. That is, the small pore pressure decrease (a few bars) tends to strengthen rather than to weaken the rock mass and thereby reduces the likelihood of induced seismicity. *Evans et al.* (2012) investigated 41 European case histories of induced seismic responses to fluid injection. In 25 cases, the injection was done into sedimentary rocks from which seven experiments were associated with felt seismicity. In eight out of 25 experiments with sedimentary rocks, injection occurred into or close to faults from which only one site produced felt seismicity, i.e. Unterhaching (*Megies and Wassermann*, 2014). In addition to the hazard of induced seismicity, it is also important to understand why geothermal seismicity is generated at some sites and is evidently absent at others.

The actual underlying physical mechanism of shear dilatation, due to injection of large fluid volumes at high pressure, however, is not yet fully understood. Depending on rock properties, injection pressure, fluid volume and temperature, res-

ervoir rocks can respond with tensile failure (hydraulic fractures; *Hubbert and Willis*, 1957), or with shear failure of pre-existing joint sets (dilatant shear; *Hubbert and Rubey*, 1959). In the oil industry, the relationship between seismic events and hydraulic fractures has been studied extensively (*Fix et al.*, 1989; *Zhu et al.*, 1996; *Dyer et al.*, 1999; *Shapiro and Dinske*, 2007; *Fischer et al.*, 2008). In geothermal activities, no matter if the HDR, EGS, or multi-fracturing concept is used the interaction of tensile and shear fractures may complicate the seis-

Table 1.
Geothermal sites analysed in the GEISER project. Maximum observed magnitude in deep crustal injection experiments listed in increasing order of local/moment seismic magnitude. Additional columns indicate rock type and stress, maximum wellhead pressure, reservoir depth, fracture mechanism, starting year of reservoir development, and references.

Sites analysed in GEISER	M_{max}^{obs}, (year)	Geology, rock type, stress	P_{max}, MPa Reservoir depth (km), fracture mechanism	Sources
The Geysers , California USA	4.6[a], 1982[c]	Metagraywacke SH-NE-SW[WSM]	7	3 km, cooling-induced shear slippage, since 1975	Oppenheimer 1986, Rutqvist et al. 2010
Berlin, El Salvador	4.4[a], 2003[c]	young volcanic weak rock, SS + NF; SH-NNW-SSE	13	2 km, opening and closing of flowing fractures, since 1991	Bommer et al. 2006, Kwiatek et al. (in this issue)
Cooper Basin, Australia	3.7[a], 2003	granite with 3.6 km sediment cover, TF; SH-EW	68	4.1–4.4 km, slip on pre-existing sub-horizontal fractures, since 2003	Asanuma et al. 2005, Baisch et al. 2006
Alkmaar, NL	3.5[a], 2001	sandstones, 2.6 to 3.1 km depth SH-NW-SE[WSM]	18	2 km, reactivation Roer Valley Rift faults, gas production since 1963	van Eijs et al. 2006, Dost and Haak 2007
Basel, Switzerland	3.4[a], 2006[c]	granite, Sh, 0.7SV, SH-N 144°E±14°	30	4.4–4.8 km, pre-existing, en-echelon-type shear zone, since 2006	Häring et al. 2008, Evans et al. 2012
Soultz-sous-Forêts, France	2.9[a], 2003	granite, NF + SS, SH-N 170°E	16	4.5–5.0 km (GPK3), single large tectonic fracture zone, since 1987	Cuenot et al. 2008, Dorbath et al. 2009, Calo et al. (in this issue)
Paralana, Australia	2.5[a], 2.4[b], 2011[c]	Hybrid, granitic basement, 4 km sediment cover, TF	62	4 km, reverse fault events	Hasting et al. 2011, Albaric et al. (in this issue)
Rosmanowes, Cornwall, UK	2.0[a], 1987	Carnmenellis granite batholite SH-NW-SE[WSM]	16	2 km, system of natural fractures, since 1977	Pine and Batchelor 1984, Trubitt et al. 1987
KTB, Germany	1.4[b], 1994	gneiss, metagabbro SS (1-8km); SH-N 160°E	53	9.1 km, scientific wells, dilatant shear cracks, since 1987	Zoback and Harjes 1997, Baisch and Harjes 2003, Jost et al. 1998
Groß-Schönebeck, Germany	-1.0[b], 2007	Rotliegend sand-stone, volcanic rock NF, SH-N 18°E	60	4.1 km, only a total of 80 seismic events detected, doublet in 2007	Huenges et al. 2006, Kwiatek et al. 2010

M_{max}^{obs}= maximum seismic magnitude observed. SH= maximum horizontal, Sh= minimum horizontal, SV= vertical in situ stress, SH-azimuth (N°E), WSM= stress orientation from World Stress Map; NF= normal, TF= thrust, SS= strike-slip faulting. P_{max} = maximum well head pressure.
[a] Local.
[b] Moment magnitude.
[c] Time and location: Basel, Upper Rhine Graben – few hours after shut-in, but before bleed-off at the edge of the cloud; Berlin, El Salvador – two weeks after shut-in; Paralana, Austalia – at the end of 2nd stimulation, at the base of seismic cloud; Soultz-sous-Forêts, Lower Rhine Graben – in 2000, 2003 and 2004 after shut-in; The Geysers, CA (USA) – on the edges of the seismic cloud.

mic footprint of a reservoir to be developed (*Jung*, 2013).

This overview article is structured according to the development of a geothermal field. In Section 2, the seismic response to fluid injected is evaluated. For this, the seismic network (borehole versus surface stations), velocity model and structural geology aspects (subsurface faults) are discussed in relation to hydraulic parameters, rock type and in situ stress regime. In Section 3, one of the most challenging aspects in the analysis of EGS seismicity is addressed, understanding the mechanisms leading to larger magnitude events (LME). Here, we discuss LME in relation to pore fluid pressure, injected volume and in the context of fault and reservoir size. Note that *Grünthal* (2014) replaces the term LME by SEECo, seismic events of economic concern. In Section 4, the maximum observed magnitude of EGS seismicity is compared to the maximum expected magnitude estimated from fault-scaling relationship, deterministic fracture models, probabilistic approaches and empirical laws.

2. Seismic response to fluid injection: network design, velocity model, hydraulic parameter and reservoir stress regime

Before a geothermal system can be exploited, it has to be assessed. During this reconnaissance phase several geophysical techniques can be used. In this section we focus on the analysis of induced seismicity as a tool to probe key parameters of the geothermal reservoir. The goal is to improve the technique of EGS, first by investigating the role of induced seismicity as an instrument to image fluid pathways generated by hydraulic stimulation treatments, and second, by addressing the consequences of hydraulic treatments for potential seismic hazard (*Bruhn et al.*, 2011). We summarize and interpret results from the analyses of various geothermal sites, located in different tectonic settings (Table 1). All of these sites have been investigated within the framework of the European Union project GEISER. In Europe, locations include the Lower Rhine Graben site in Soultz-sous-Forêts, France (*Evans et al.*, 2005), the Upper Rhine Graben site in Basel, Switzerland (*Häring et al.*, 2008), Icelandic geothermal test sites (*Jousset et al.*, 2010, 2011), Latera (Italy) and Groß Schönebeck in the North German Basin (*Kwiatek et al.*, 2010). Non-European sites investigated include Berlin, El Salvador (*Bommer et al.*, 2006; *Kwiatek et al.*, 2014), The Geysers in California, USA (*Oppenheimer*, 1986; *Majer et al.*, 2007), Cooper Basin (*Asanuma et al.*, 2005; *Baisch et al.*, 2006) and Paralana (*Hasting et al.*, 2011; *Albaric et al.*, 2014), both in Australia and Bouillante in Guadeloupe (*Sanjuan et al.*, 2010; *Calcagno et al.*, 2012). Two reference sites were included, where seismicity was induced by other than geothermal causes. At the KTB deep drilling site, injection of 200 m³ of brine in a stable continental region produced low magnitude seismicity (*Zoback and Harjes*, 1997; *Baisch and Harjes*, 2003), and in The Netherlands (NL) the induced seismicity is related to gas production (*van Eck et al.*, 2006; *Dost and Haak*, 2007; *van Wees et al.*, 2014).

The analysis of seismic data from various EGS stimulations shows that a clear relationship exists between fluid injection and seismic response represented by the maximum observed magnitude at each site. Fig. 1 displays the observed maximum magnitude of seismic events as a function of injected fluid at EGS sites (Table 2) in comparison to data from wastewater disposal wells, hydraulic fracturing operations and scientific drilling projects (*McGarr*, 2014). It is apparent that the maximum observed magnitude increases with increasing volume of injected fluid. The comparison between wastewater disposal wells (Fig. 1, triangles from *McGarr*, 2014) and geothermal operations (Fig. 1, squares) indicates that the latter involve
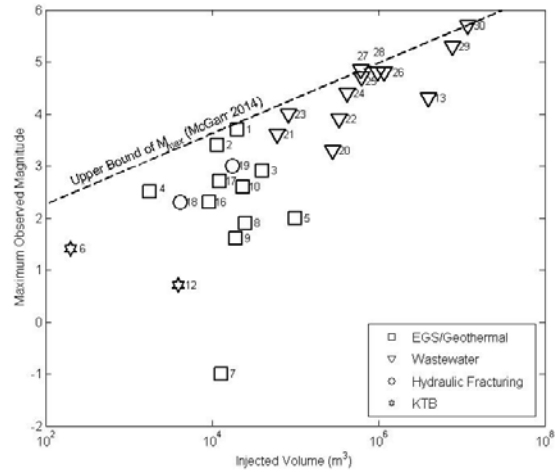
Figure 1. Observed maximum magnitude of seismic events in geothermal operations (squares), wastewater disposal wells (triangles), hydraulic fracturing (circles), and fluid injection in the KTB scientific well (stars) as functions of volume of injected fluid. Numbers by symbols correspond to the order in which data are listed in Table 2.

less fluid volume while smaller maximum magnitudes are observed. Lower-bound values come from KTB stimulations (Fig. 1, stars #6 and #12) and the Groß Schönebeck geothermal site (Fig. 1, square #7). In Fig. 1, the dashed line (from *McGarr*, 2014) appears to define an upper bound to the data.

A widely observed feature in the spatiotemporal distribution of seismicity is a gradual migration from the vicinity of the borehole to distances farther from the borehole as fluid injection is progressing. In many cases as injection proceeds seismicity continues throughout the volume rather than in an expanding ring. This has implications on the rate of permeability creation. The ability to track details in the spatiotemporal distribution of seismicity and its source parameters, however, depends primarily on the quality and the configuration of the seismic network, on the quality of the velocity model and on the applied algorithms to invert for event locations.

The total extension of the seismic network and the configuration of the seismic stations influence the completeness and accuracy of the event locations. Networks that include single borehole sensors or strings of deep borehole three-component sensors can detect and locate more events at a lower magnitude threshold than networks that consist solely of surface stations. This is primarily due to the shorter distances between the sensors and the event locations, and to avoiding the heterogeneous and attenuating near surface layers, as well as to the improved signal-to-noise ratio from being below the surface. This results in reduced amplitude losses from geometrical spreading and intrinsic and scattering attenuation, as observed when comparing data from deep borehole with surface seismic data (*Oye et al.*, 2004). Near-surface low-Q sedimentary layers (see Table 1, Groß Schönebeck), are particularly detrimental to the recorded signal quality, especially for *S*-wave arrivals (*Oye et al.*, 2010). Strong impedance contrasts between the surface and the injection level can add complexity in the wave-form data, such as *S*-to-*P* wave converted phases (e.g., observed in Basel by *Deichmann et al.* (2014) and in Paralana by *Albaric et al.* (2014)). Such interfaces complicate the waveforms and thereby automatic data processing (phase arrival picking and identification), focal mechanism determination (*Deichmann et al.*, 2014) and full moment tensor inversion (*Zhao et al.*, 2014). In general, the shorter the travel paths the simpler the wave-forms, which results in better constrained source inver-

Table 2.
Extended field data including EGS/geothermal data, wastewater disposal, hydraulic fracturing and KTB stimulation. Columns indicate maximum observed magnitude, maximum wellhead pressure, depth of reservoir, maximum inflow, total injected volume, reservoir type, stress regime (NF, SS, TF) and references.

#	Name/location	M_{max}^{obs}	P_{max} (MPa)	Depth (km)	Q_{max} (l/s)	V_{tot} (m³)	Res. type	Stress regime	Sources
1	Cooper Basin	3.7	68	4.25	24	20,000	1	TF	Asanuma et al. (2005), Baisch et al. (2006)
2	Basel	3.4	30	4.6	62	11,570	1	SS	Häring et al. (2008), Evans et al. (2012)
3	Soultz-Sous-Forêts, deep reservoir stimulation GPK3	2.9	16	4.75	50	39,800	1	NF/SS	Cuenot et al. (2008), Dorbath et al. (2009), Calo et al. (this issue), Baisch & Vörös (2009), McGarr (2014)
4	Paralana	2.5	62	4	19.8	1,800	1	TF	Hasting et al. (2011), Albaric et al. (this issue)
5	Rosmanowes	2.0	16	2	100	100,000	1	SS	Pine & Batchelor (1984), Turbitt et al. (1987)
6	KTB 1994	1.4	53	9.1	9	200	4	SS	Zoback & Harjes (1997), Jost et al. (1998), Baisch & Harjes (2003)
7	Gross Schönebeck	-1.0	60	4.2	150	13,000	1	NF	Huenges et al. (2006), Kwiatek et al. (2010)
8	Soultz-sous-Forêts upper reservoir, GPK1, 1st stimulation	1.9	11.4	3	36	25,300	1	NF/SS	Baisch & Vörös (2009)
9	Soultz-sous-Forêts upper reservoir, GPK1, 2nd stimulation	1.6	10	3	50	19,300	1	NF/SS	Baisch & Vörös (2009)
10	Soultz-sous-Forêts deeper reservoir GPK2	2.6	15	4.7	51	23,400	1	NF/SS	Baisch & Vörös (2009)
11	Genesys Horstberg	-	34	3.79	50	20,100	1	TF	Baisch & Vörös (2009)
12	KTB 2000	0.7	30	5.4	1.17	4,000	4	SS	Baisch & Vörös (2009)
13	Paradox Valley	4.3	34.5	4.3	17.5	4,000,000	2	TF	Baisch & Vörös (2009)
14	Soultz-sous-Forêts upper reservoir GPK2	-	12.3	3.6	56	28,000	1	NF/SS	Baisch & Vörös (2009)
15	Soultz-sous-Forêts upper reservoir GPK2, re-stimulation	-	15.3	3.6	79	27,500	1	NF/SS	Baisch & Vörös (2009)
16	Soultz-sous-Forêts deeper reservoir GPK4	2.3	17	4.75	30	9,300	1	NF/SS	Baisch & Vörös (2009)
17	Soultz-sous-Forêts deeper reservoir GPK4, re-stimulation	2.7	18	4.75	45	12,300	1	NF/SS	Baisch & Vörös (2009)
18	Bowland Shale, UK	2.3	55		191	4,170	3	SS	McGarr (2014), de Pater & Baisch (2011)
29	Garvin County, OK	3.0				17,500	3	SS	McGarr (2014)
20	Dallas Fort-Worth Airport, TX	3.3	13.6	3.75	18.4	282,000	2	NF	McGarr (2014), Frohlich et al. (2011)
21	Ashtabula, OH, July 1987	3.6	28.4	1.9	1.9	61,700	2		McGarr (2014), Nicholson & Wesson (1990)
22	Ashtabula, OI, January 2001	3.9				340,000	2		McGarr (2014), Nicholson & Wesson (1990)
23	Youngstown, OH	4.0	17.2		10	83,400	2	SS	McGarr (2014), Kim (2013)
24	Raton Basin, CO, Sept. 2001	4.4	6.2			426,000	2	NF	McGarr (2014), Meremonte et al. (2002)
25	Guy, AR	4.7	20.3		27.6	629,000	2	NF	McGarr (2014), Horton (2012)
26	Painesville, OH	4.8				1,190,000	2	SS	McGarr (2014)
27	Denver, CO	4.85	7.6		25.2	625,000	2	NF	McGarr (2014), Herrmann et al. (1981), Hsieh & Bredehoeft (1981)
28	Timpson, TX	4.8	17	1.9	16.5	991,000	2	SS	McGarr (2014), Frohlich et al. 2014
29	Raton Basin, CO, August 2011	5.3				7,840,000	2		McGarr (2014)
30	Prague, OK	5.7	3.6	1.7	0.6	12,000,000	2	SS	McGarr (2014), Keranen et al. 2013

M_{max}^{obs} = maximum seismic magnitude observed; P_{max} = maximum well head pressure; Q_{max} = maximum inflow; V_{tot} = total volume of injected fluid; reservoir type: (1) EGS/geothermal, (2) wastewater, (3) hydraulic fracturing, (4) KTB; stress regime: NF= normal, SS= strike-slip, TF= thrust faulting

sion due to Green's functions that reveal less complexity.

In the case of EGS, economic reasons often prevent extensive downhole monitoring systems and additional surface stations or a combination of deep and shallow borehole stations might be considered. An additional important factor is the location of the planned EGS site, as the influence of cultural noise varies significantly between densely populated areas, as in the case of Basel, and remote places with insignificant noise sources such as the Australian bushlands in the environs of Paralana. Depending on the noise conditions, different depths for borehole sensors might be advisable to achieve an optimized ratio of noise reduction and costs. E.g., *Majer et al.* (2008) found a 60 dB improvement in signal-noise ratio at depth over ca. 152 m. In any case, we recommend inclusion of a surface network to enhance the azimuthal coverage required for the determination of source mechanism and to ensure that the seismic events are within the footprint of the network. For example the seismic network in Basel consists of six deep borehole stations with one three-component sensor deployed in each borehole, in addition to an extensive surface seismic network. *Kraft and Deichmann* (2014) investigated how to improve the catalogue of about 3500 events using cross-correlation methods and high-quality downhole data. They also compare estimated focal mechanisms from the downhole network with focal mechanisms based on data from the surface network. Of the 3500 events recorded and located by the borehole network, less than 200 were detected by the surface stations. The minimum magnitude and the magnitude of completeness of the surface data were M_w 0.9 and 1.5, in contrast to M_w 0.1 and 0.8 for the borehole data.

A critical factor for successful location of microseismic events is the quality of the P-wave and S-wave velocity models. Shear-wave velocities are often extrapolated from simple P-wave velocity models (*Castagna et al.*, 1985), resulting in high uncertainties in the event locations. *Albaric et al.* (2014) discussed the importance of obtaining a good understanding of the local structural geology before the main stimulation phase. In their paper about hydraulic stimulation at the Paralana EGS in Australia, the authors took advantage of several 2D seismic lines and additional information from borehole logs to construct 3D velocity models for P-and S-wave velocities, which were subsequently used to locate the seismic events. The knowledge of the velocity models remains important during source parameter determination, derivations of Green's functions for moment tensor calculation and temporal changes of the velocity models due to EGS operations (Fig. 2). Positive temporal correlation between injected fluid volume and Vp/Vs-ratio was observed at The Geysers by *Gritto and Jarpe* (2014). *Calò et al.* (2011) interpreted Vp anomalies observed during stationary injection conditions at Soultz-sous-Forêts as being caused by effective stress variations linked to fluid diffusion. Fast changes of wave velocities associated with flow rate changes were interpreted by aseismic motions within the reservoir.

In some cases, for instance, the Bouillante geothermal field, Guadeloupe, French Antilles, little seismicity is associated with the geothermal exploitation and therefore seismicity cannot be used for reservoir characterization (*Sanjuan et al.*, 2010). Recently, ambient seismic noise analysis has been successfully applied to image velocity structures even in the absence of seismicity (e.g., *Clarke et al.*, 2013). This technique can be used to retrieve information about structural features of the reservoir, which can subsequently be used to highlight relative velocity changes and also to identify possible regions of aseismic slip. It is important to note that such data need to be acquired before the first stimulation phase, so that baseline data are available for later comparison. Modelling should be used to optimize the network geometry for this method.

Today's EGS reservoirs, developed between 2 and 5 km
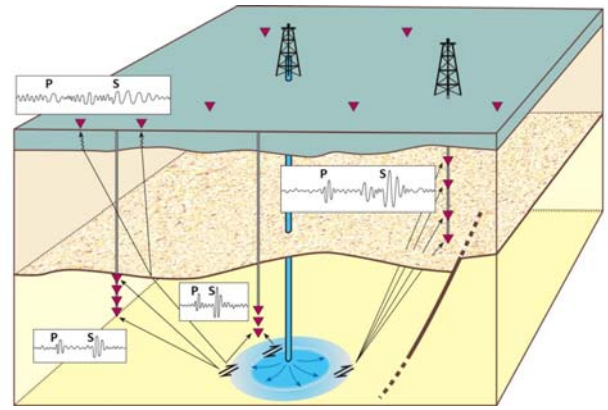
Figure 2. Sketch of potential seismic networks to monitor seismicity related to a hydraulic stimulation at depth. Schematic waveform examples are shown for four different scenarios: closely placed downhole sensors show the highest quality **P** and **S** wave onsets, whereas for surface seismic sensors the observed amplitudes may suffer from attenuation, high-impedance contrasts that introduce secondary or converted phase arrivals and higher noise levels. (For interpretation of the references to colour in this figure legend, the reader is referred to the web version of the article.)

depth (Tables 1 and 2), do not exhibit a relationship between the number of recorded events or the maximum magnitude and reservoir depth (*Evans et al.*, 2012). However, the depth of the reservoir needs to be taken into account when it is linked to the injection pressure and to the crustal stress state. In Fig. 3, hydraulic reservoir parameters are displayed in combination with the tectonic stress regime. As such, the maximum inflow of the reservoir is plotted as a function of the maximum wellhead pressure for geothermal sites (squares), waste disposal wells (triangles) and the KTB scientific drilling site (stars). For example, the Soultz-sous-Forêts EGS site (Fig. 3, square #15) is characterized by high inflow and low wellhead pressure in a normal faulting regime. On the other hand, the Cooper Basin EGS site (Fig. 3, square #1) shows low inflow and high wellhead pressure values in a thrust faulting regime. Wastewater disposal wells are characterized by low maximum inflow values (Fig. 3, triangles). Like in Fig. 1, the Groß Schönebeck datum (square #7) is sitting outside the boundary of most of the data indicated by the solid line.

Pre-stimulation seismic monitoring might be useful to identify buried faults and before installation of borehole seismometers in observation wells. Well-logging and well testing is recommended to gather information on the seismic velocity distributions and on the in situ stress conditions, which may provide better constraints to extrapolate to actual reservoir stress conditions.

3. Source mechanism of larger magnitude events (LME) and their occurrence in space and time in the stimulation phase

In the stimulation phase of EGS, high pressure fluid is pumped into the rock formation to generate fracture networks needed for heat exchange. Hydraulic parameters measured include temperature of injected water, fluid inflow rate and wellhead pressure. We introduce the scalar quantity injectivity (I), which is defined by the ratio of maximum inflow rate to maximum wellhead pressure to characterize the reservoir. Note that in oil and gas exploration, the injectivity index (II) is obtained from field tests upon completion of wells, and its computation requires a more sophisticated approach. In general, injectivity describes the capacity of a well or formation to accommodate pumped-in fluid. Injectivity tests are conducted to establish the rate and pressure at which fluids can be
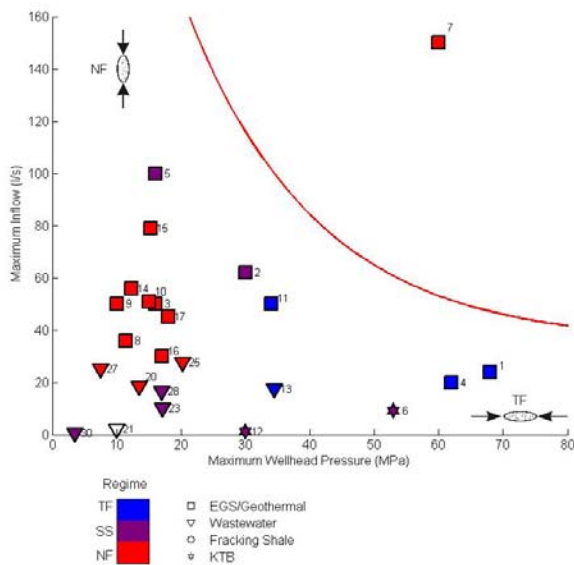
Figure 3. Hydraulic parameters in the reservoir displayed together with the tectonic stress regime. Maximum inflow is plotted as a function of maximum wellhead pressure for fluid-injection field experiments from Fig. 1. Symbols are colour coded according to stress regime prevailing at target depth (red = normal-, purple = strike-slip-, blue = thrust faulting). Insets indicate elongation of the seismic cloud in the direction of maximum principal stress. (For interpretation of the references to colour in this figure legend, the reader is referred to the web version of the article.)

Figure 4. Observed maximum magnitude of induced seismic events as a function of injectivity of the reservoir (ratio of maximum injection rate and maximum wellhead pressure) computed from Table 2 data. Line indicates upper boundary trend with one exception, the Rocky Mountain Arsenal wastewater disposal (#27). Lower limit datum represents the Groß Schönebeck geothermal site (#7).

pumped into the treatment target without fracking the formation. Computing the injectivity index II is the most common way of analysing performance of injection wells. The computation includes injection rate, injection pressure corrected for bottom hole flow conditions, and far-field reservoir pressure (e.g., *Economides and Saputelli*, 2005). In the following, the simple injectivity definition *I* is used instead of the injectivity index *II* because of lack of data. In Fig. 4, reservoir injectivity I is plotted as a function of maximum observed seismic magnitude. Apart from the data collected at the Rocky Mountain Arsenal wastewater disposal site (Fig. 4, #27), disposal wells are characterized by lower injectivities ($I < 1.5$) compared to most EGS sites. This seems counter intuitive to what one would desire in a wastewater disposal well but may be explained by the fact that for EGS sites the injectivity computation is conceptually problematic. This is because one has to correct for dynamic (fluid-driven) fractures, which is required in EGS stimulation. In our simple approach, EGS sites (Fig. 4, squares) indicate a wide range of injectivity values from 0.32 (Fig. 4, #4, Paralana) to 6.25 (Fig. 4, #5, Rosmanowes) with LME ranging from −1 to 3.7 (Fig. 4, #7 and #1). For comparison, the observed maximum seismic magnitudes in wastewater disposal range from 3.3 (Fig. 4, #20) to 5.7 (Fig. 4, #30). The solid line is an upper boundary to most of the data, except for the wastewater disposal at Rocky Mountain Arsenal (Fig. 4, #27). The Groß Schönebeck datum (Fig. 4, #7) indicates the lower limit.

One major topic addressed by a number of papers is the characterization of LME, coupled with the investigation of strategies to assess and, ideally, mitigate seismic hazard associated with stimulation operations. As seismicity is induced in the process of enhancing or creating the permeability, it is important not to induce or to trigger LME, which may not only cause damage at the surface, but also might lower the efficiency of the geothermal system through the creation of high-permeability pathways. If a LME occurs, it may create a master
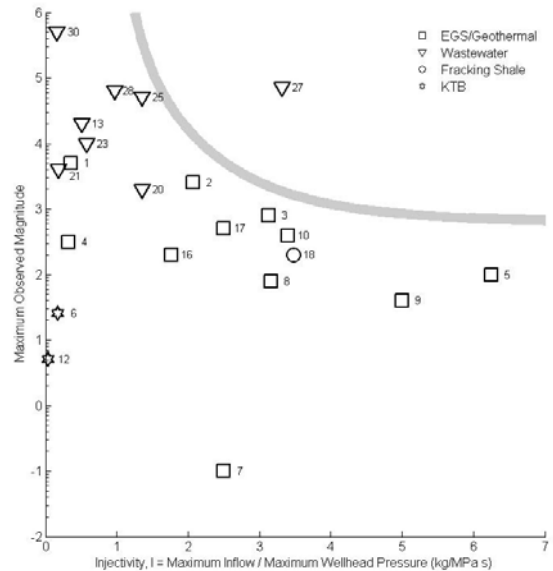
pathway for fluids, preventing efficient heat exchange. A better physical understanding of the reservoir- and seismicity generation process is needed in order to develop techniques to reduce the probability of occurrence of LME.

It was first proposed by *McGarr* (1976) that the total moment of an induced seismic cloud is proportional to the volume of injected fluid, see Fig. 1. However, the actual amount of seismicity (or the proportionality factor) can vary substantially between different reservoirs for similar injected fluid volumes. Using a completely different approach of pressure diffusion theory, *Shapiro et al.* (2007, 2010) obtained a similar result in which the total number of induced events is proportional to the injected fluid volume. In addition, they describe the proportionality factor, the seismogenic index, as a function of measurable seismological quantities and rock properties. Combining these considerations with the assumption that seismicity always follows a Gutenberg–Richter-type magnitude distribution leads to a probabilistic estimate of the maximum expectable magnitude.

The conclusion is that the probability of a LME generally increases with injected volume, even though there are significant regional differences. For this reason, we shall differentiate between long-term injection operations (e.g., wastewater disposal (triangles in Figs. 1, 3 and 4) or CO_2 disposal) where large (net) volumes may accumulate over time, and the short-term stimulation operations at the beginning of an EGS project (squares in Figs. 1, 3 and 4). Most of the LME reported in the literature have occurred either after long-term fluid injection (*Ake et al.*, 2005; *Frohlich et al.*, 2011, *McGarr*, 2014), or as a result of reservoir impoundment (*Gupta*, 2002, 2011), both of which can bring pre-existing fractures in the shallow crust closer to failure. Of the short-term stimulation activities, EGS stimulations have generally shown a much higher propensity to produce LME, compared, e.g., to hydraulic fracturing in the oil- and gas industry. *Shapiro et al.* (2010) find significantly higher seismogenic indices for geothermal stimulations in crystalline rocks than for comparable operations in sedimentary formations. Similarly, *Evans et al.* (2012) suggested that injection into sedimentary rocks tends to be less seismogenic

than into crystalline rocks. Also from laboratory testing it is known that acoustic emission activity and source mechanisms are very different for e.g., sandstones (*Lockner and Byerlee*, 1972; *Zang et al.*, 1996) as compared to granite (*Lockner and Byerlee*, 1992; *Zang et al.*, 2000). This is caused by different fracture mechanisms operating during fluid injection into different rock types as discussed in Section 5.

Large or damaging earthquakes tend to occur on developed or active fault systems. In other words, large earthquakes are unlikely to occur in absence of a fault large or long enough to release considerable energy. *Evans et al.* (2012) compare the maximum magnitude observed at each project with the regional seismic hazard expressed in terms of the long-term probability of exceeding threshold peak ground acceleration (PGA), and they speculate that fluid injection in areas with lower natural seismicity may have a lower risk of triggering LME. However, a causal relationship if any between the two properties (maximum magnitude and PGA threshold level) remains unclear and requires a more detailed geomechanical examination of each project (see Section 4).

Table 1 lists GEISER related sites with the largest LME in decreasing order of event magnitude. Some of these cases, mainly Basel (Switzerland), Soultz-sous-Forêts (France), Paralana (Australia) and Berlin (El Salvador), were studied in detail as part of the GEISER programme. In addition to magnitudes (moment magnitudes wherever available), the time and location of recorded LME at these sites are listed in the text below Table 1. As stated before, it has been frequently observed that LME occur after shut-in and at larger distances from the injection well (*Baisch et al.*, 2010).

3.1 Berlin, El Salvador

Kwiatek et al. (2014) present a case study on the geothermal project in Berlin, El Salvador, where a $M_w = 3.6$ LME occurred two weeks after shut-in of the injection in the central part of the reservoir ca. 2 km away from the injection well using relocated data. They found that the seismic activity induced by multiple injections into well TR8A did not reach distances longer than 500 m from the injection point. They do not observe any sequence of events migrating further away towards the nucleation of the LME. However, the multiple injection operations at TR8A can be responsible for changing dominant fluid migration pathways, and indirectly may be responsible for the occurrence of LME in the Berlin geothermal field. They also found a dependence of stress drop on distance from the injection point, somewhat similar to what was found by *Goertz-Allmann et al.* (2011) for Basel, but not nearly as well defined.

3.2 Paralana, Australia

In Paralana, Australia, during a stimulation in July 2011, four LME with $M_w = 2.4$-2.5 occurred during periods of massive injection. As shown by *Albaric et al.* (2014), the hypocentres of the first three of these events were located at the periphery of the extent of the seismic cloud at that time, whereas the fourth occurred closer to the well, in a zone which had experienced activity earlier during the stimulation process (Fig. 5).

3.3 Soultz-sous-Forêts, France

The EGS at Soultz-sous-Forêts, France, has a long history of stimulation and circulation through several wells at different depths. A short summary of the activities can be found in *Evans et al.* (2012). A stimulation in 1993 at depths of 3–3.5 km produced only minor seismic activity, with a maximum magnitude of 1.9. Subsequently, three additional wells, GPK2, GPK3 and GPK4, were drilled to depths of 4.5–5 km. GPK2 was
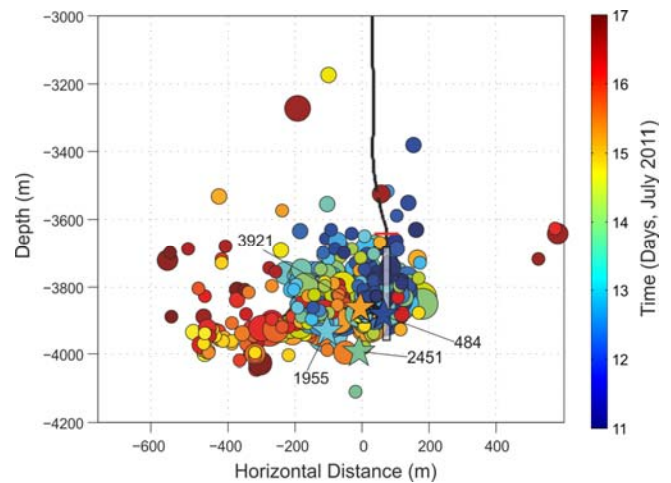
Figure 5. Nearly North–South trending depth-cross-section through the seismic cloud induced during the stimulation of the Paralana EGS (modified from *Albaric et al.*, 2014). The symbols are color-coded according to the time of occurrence of each event and their size is proportional to the magnitude ($0.5 \leq M_w \leq 2.5$). The numbered stars correspond to the four LME with M_w in the range 2.4–2.5. (For interpretation of the references to colour in this figure legend, the reader is referred to the web version of the article.)

stimulated in June 2000, GPK3 in May 2003 and GPK4 in September 2004 and February 2005. Events with magnitudes as high as 2.5 were recorded during the stimulation of both GPK2 and GPK3, and in each case, the strongest event occurred after shut in – a magnitude 2.6 event some 10 days after shut-in of GPK2 and two magnitude 2.9 and 2.7 events three-and-a-half and five days after shut-in of GPK3 (*Dorbath et al.*, 2009). The stimulation of GPK4 occurred in three phases – the first two as conventional freshwater injections and the third with the addition of acid. A total of four events with magnitudes greater than 2 were induced by these activities: during the first phase, a magnitude 2.3 event occurred a few hours after injection was stopped; during the second phase, a magnitude 2.7 event occurred at the height of the injection; during the third phase, a magnitude 2.2 event occurred during stimulation and a magnitude 2.3 event occurred about eight days later, when both the well-head pressure and the seismic activity had declined to almost normal levels again. *Dorbath et al.* (2009) showed that the relative size distribution of earthquakes, as expressed by the *b*-value of the Gutenberg–Richter relation, was significantly different for the events induced during the stimulation of GPK2 and GPK3: whereas the average *b*-value was around 1.23 at GPK2, it was only 0.94 at GPK3. The difference seems to be linked to the observation that the seismic cloud induced at GPK2 is diffuse and structureless, whereas at GPK3 the hypocentres align along major faults that can be traced back to the wells, where they were identified in the borehole logs. Furthermore, *Dorbath et al.* (2009) reported that the two 2003 events with magnitude 2.9 and 2.7 were located on two of these major faults.

3.4 Basel, Switzerland

One of the most intensively studied EGS stimulations that triggered several LME causing damage at the surface is the project in Basel, Switzerland. In Basel the largest magnitude event ($M_L = 3.4$) occurred a few hours after shut-in but shortly before the well was opened, while three additional events with $M_L > 3$ occurred one to two months later, long after the well-head pressure had dropped to near-normal levels. The hypocentres of these earthquakes were located at the periphery of the seismic cloud. Several studies have observed that a large percentage of the seismicity induced by the Basel EGS
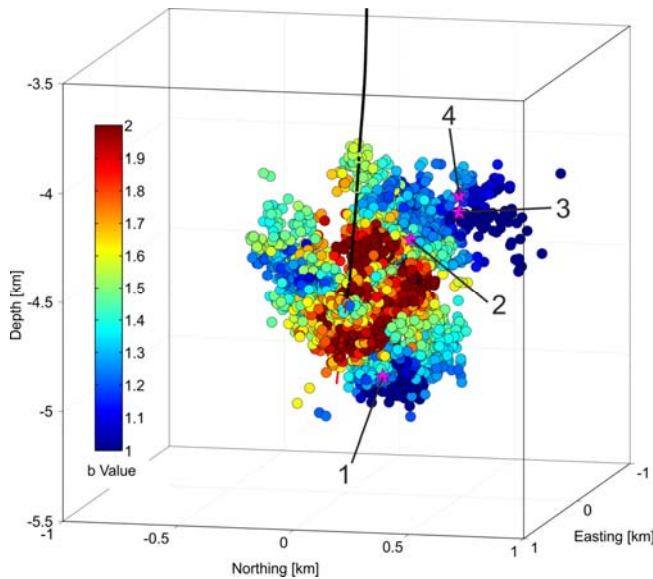
Figure 6. The seismic cloud induced by the stimulation of the Basel EGS in 2006 and 2007. The hypocentres are colour coded according to the **b**-values calculated for the rock volume in which they occurred (modified from *Bachmann et al.*, 2012).While values range from M_w 0.8 to 3.5, the colour bar is limited from 1 to 2 for a clearer visibility. The stars correspond to the four LME with $M_L \geq 3$ (1: 2006/12/08, $M_L = 3.4$; 2: 2007/01/06, $M_L = 3.1$; 3: 2007/01/16, $M_L = 3.2$; 4: 2007/02/02, $M_L = 3.2$).(For interpretation of the references to color in this figure legend, the reader is referred to the web version of the article.)

occurred in clusters of similar events, which implies that their hypocentres are located close to each other and that their focal mechanisms are nearly identical (e.g., *Deichmann et al.*, 2014 and references therein). In other words, it seems that earthquakes within these clusters of similar earthquakes occur on the same faults. Results of high-precision relative locations of the events within such clusters show that their hypocentres define near-planar structures that coincide with one of the nodal planes of their focal mechanisms. Detailed analyses of the sequences associated with the larger magnitude events ($M_w > 2$) induced during the stimulation of the Basel EGS showed that the activated faults have dimensions of the order of several 100 m and are often oriented obliquely to the overall trend of the microseismic cloud (*Deichmann et al.*, 2014). These results reveal a complex internal structure of the flow paths in the rock volume stimulated by the water injection and imply that geomechanical models consisting of a single through-going structure are not realistic.

One of the key discoveries of the research performed on the seismicity induced by the Basel EGS concerns the relative size distribution of the induced earthquakes. The results of a high-resolution b-value mapping by *Bachmann et al.* (2012) are summarized in Fig. 6, which shows the highly-systematic spatial heterogeneity of the b-values associated with the seismicity induced by the Basel EGS. Unusually high b-values shown in red are found near the injection point and earlier in the sequence; further out, b-values tend to be closer to the normal tectonic average of around 1.0. A small b-value is equivalent to a higher probability for the occurrence of larger-magnitude events and is consistent with the observation that the largest induced seismic events often – but not always – occur after shut-in and at the periphery of the stimulated rock volume. Indeed, as shown in Fig. 6, the hypocentres of the four largest events are located in regions of low b-values.

The size distribution of fractures in rock is a power function of fracture size and the exponent of this relation scales inversely with stress. Based on *Mogi* (1962) laboratory acoustic emission studies on heterogeneous materials and its rela-

tion to earthquake phenomena, *Scholz* (1968) highlighted that the b-value of magnitude frequency distributions (grain-scale cracks or earthquakes) strongly depends on the state of stress. Recent laboratory measurements and also regional b-value estimates have shown that b-values are inversely proportional to the differential stress and thus may qualitatively be used as stress indicators at depth, where generally no direct measurements are available (*Amitrano*, 2003; *Schorlemmer et al.*, 2005). Assuming that earthquakes occurring in regions of high differential stress or on faults with large shear stresses, on average tend to have higher stress drops, one should expect a systematic spatial variability of earthquake stress drops similar to the variability observed for the b-values. In fact, the stress drops determined by *Goertz-Allmann et al.* (2011) for the induced seismicity of Basel vary over a wide range and tend to increase systematically with distance from the injection point and, thus, with time.

Zhao et al. (2014) analysed the 19 largest events that occurred during and after the injection sequence and determined moment tensors from full waveforms. That analysis resulted in similar double-couple components as found by *Deichmann and Ernst* (2009). In addition, it revealed significant isotropic components during the early injection phase, whereas most of the events in the later stage are dominated by double-couple components. Their result implies sizeable volume changes caused by large pore pressures at the early times close to the injection, consistent with the pore pressure estimates of *Terakawa et al.* (2012). Isotropic moment tensor components may relate to the occurrence of long-period events (*Bame and Fehler*, 1986; *Ferrazzini et al.*, 1990; *Jousset et al.*, 2010). The locations of the events with high isotropic components also coincide with previously found regions of high b-values (*Bachmann et al.*, 2012) and low stress drops (*Goertz-Allmann et al.*, 2011).

All of these observations provide a consistent picture in the near- and far-field of the stimulation well. Early during the stimulation phase and close to the injection well, pore pressures are high (near-field). Here many small events, often on faults with low applied shear stress, are induced, consistent with the high b-values, low stress drops and significant volumetric components of the focal mechanisms. As the injected water migrates away from the injection point and the pore pressure decreases (far-field), the volumetric component of the focal mechanism becomes insignificant and the shear stress necessary to trigger an event must increase. This is reflected in higher stress drops and in lower b-values. The latter implies a higher probability for the occurrence of the often-observed larger magnitude events at the periphery of the stimulated volume and during the later stages of the stimulation.

4. Maximum observed and expected seismic magnitude

In this section, it is important to distinguish between the maximum observed seismic magnitude (M_{max}^{obs}) at a given geothermal site (see Tables 1 and 2), and the maximum expected (or possible) magnitude (M_{max}) as typically used in probabilistic seismic hazard assessment, e.g. *McGuire* (2004) and *Kijko* (2004). While M_{max}^{obs} represents the maximum magnitude of an induced seismic event during the development of a geothermal reservoir (exploration, stimulation, circulation), M_{max} stands for the very rare seismic event happening only every thousand or ten thousand years, and is difficult to be estimated based on observed data (*Holschneider et al.*, 2014). This is because the observation periods in geothermal reservoirs (Table 1, decades) are much too short to sample M_{max}. Therefore, using M_{max}^{obs} instead of M_{max} to assess the seismic

hazard of a given site will result in an underestimation (lower limit value only). Many efforts have been made to anticipate the size and rate of occurrence of earthquakes. In the structural geological approach, the maximum magnitude is inferred from the largest potentially active fault in the geothermal reservoir (e.g., *Majer et al.*, 2007). Assigning a maximum earthquake magnitude to a given fault is based on empirical relations between magnitude and fault parameters such as length, width and displacement, as discussed by *Wyss* (1979) and *Wells and Coppersmith* (1994).

In Fig. 7, an earthquake fault relationship, after *Leonard* (2010), is shown modified for maximum observed magnitudes at geothermal sites (green stars) and tectonic earthquakes (red stars). Formulas used to prepare this figure and references are listed in Table 3. Earthquake magnitude, fault size and rupture energy increase from left to right (Fig. 7). Different rows indicate peak ground velocity (PGV), peak ground acceleration (PGA) and their relation to macroseismic intensity and moment magnitude, and their scaling with fault-related parameters like slip (D), rupture length (L) and rupture energy. For a geothermal reservoir, the problem is to downscale these empirical relations to the much smaller size of fractures expected to be created or reactivated, about 50–500 m in length (Section 3 and Fig. 7, green stars). This downscaling can be performed by a number of ways and should take into account non-linearity that may exist in the scaling laws (*Douglas and Jousset*, 2011). Although typical reservoir faults may not be detectable by 3D seismic reflection they might be able to generate seismicity with local magnitudes between 3 and 4, depending on the stress drop (*Evans et al.*, 2012).

Apart from this structural geological approach, there are other methods to estimate the maximum magnitude: (1) The deterministic approach, (2) the probabilistic approach, and (3) the empirical approach. In the deterministic approach, the generation and propagation of fluid-filled fractures when a geothermal reservoir is simulated must take into account geometry, rock properties and in situ stresses. In this approach, fracture distributions can be prescribed (*Bruel*, 2007; *Baisch et al.*, 2010; *Wassing et al.*, 2014), or dynamic crack growth models can be used (*Hazzard and Young*, 2004). For example, in *Baisch et al.* (2010), crack distributions are prescribed and slip occurs on critically stressed slider-spring patches. This model consists of a subvertical fault zone (3 km × 3 km in size) with constant pore pressure (48 MPa), which is subdivided into smaller slip patches (20 m × 20 m in size) and intersected by a well at a depth of 4.8 km (Soultz-sous-Forêts scenario). By analysing hydraulic overpressure distributions inside the fault zone as a function of radial distance to the injection well, *Baisch et al.* (2010) identified the slip patches of LME with zones of increasing overpressurization after shut-in. In this model, therefore, LME were explained by non-stationary fluid pressure conditions during EGS injections. After pumping stops, the pressure diffusion continues and the outer boundary of the reservoir, depicted by the seismic cloud, becomes subject to higher in situ pressures than before. This may cause a larger spatial area concurrently to become over-critically stressed, which tends to result in larger magnitude events. Since moment magnitude is proportional to the logarithm of the source area times the average slip, M_{max} can be estimated from the maximum size of the induced seismic cloud as a function of time from the start of the injection (See approach (3) below). This is based, however, on the assumption that the rupture surface of the largest event is limited by the size of the stimulated rock volume at a particular time, and M_{max} estimated in this way is highly sensitive to the adopted source model and assumed static stress drop. According to the model by *Baisch et al.* (2010), the maximum magnitude is controlled by the area over which fluid pressure increase brings the state of stress of the rock mass close to failure.

Increasing the area of fluid pressure will increase M_{max} during stimulation with increasing injection time. Consequently (assuming constant injection pressure), the observed seismicity migrates away from the injection well.

A dynamic fracture-growth approach is the discrete fracture network model by *Yoon et al.* (2014) (see Fig. 8). In this hydromechanical coupled model of fluid injection in a naturally-fractured reservoir, fractures are present before stimulation (Fig. 8a, lineaments), and new fractures can be formed indicated by induced seismic events during (Fig. 8b, grey dots) and after stimulation treatment (Fig. 8c, red dots). The fracturing process operates in mixed-mode. This means that pre-existing fractures can behave as tensile cracks (mode I) or hydroshears (mode II), but also new fractures can form from existing ones, e.g. as wing cracks (mode I) from existing shear crack tips (mode II). The goal is to identify the size and overall orientation distribution of existing and newly created fractures during EGS stimulation and operation, and their relation to the three principal stresses in order to optimize reservoir productivity and to reduce induced seismicity at the same time. Dynamic fracture distributions allow computation of seismic moment tensors and radiated seismic energy for comparison with hydraulic energy injected into the EGS system (*Zang et al.*, 2013). Seismic catalogues for various stimulation scenarios in dynamic fracture growth models can be used for hazard assessment of specific sites and stimulation treatments (*Hakimhashemi et al.*, 2013, 2014).

In approach (2), the probability of occurrence of an earthquake with a chosen M_{max} is derived from the magnitude-frequency distribution of earthquakes, the Gutenberg–Richter law. This requires an earthquake catalogue that spans a wide range of magnitudes. In addition, a truncation of the Gutenberg–Richter relation and thus the definition of the locally valid M_{max} value generally need additional assumptions about the tectonics and rock mechanical processes that cause the earthquakes. To this end, *Shapiro et al.* (2010) modified the Gutenberg–Richter law by introducing a tectonic potential, and computed a characteristic scalar quantity of reservoir fluid stimulation, the seismogenic index (cf. Section 3). The seismogenic index may vary between different wells of the same field or even within one well for different stimulation scenarios. In order to guide reservoir operations, we recommend computing indices to quantify seismic reservoir behaviour as a function of time, in particular in the stimulation and production phase of a reservoir.

Hakimhashemi et al. (2013) used a hybrid approach for computing induced seismicity. They started from a geomechanical model (approach 1) and applied probabilistic techniques to compute seismic hazard (approach 2). To our knowledge this was the first attempt to link approaches (1) and (2). Time-dependent Gutenberg–Richter a-value and b-value curves computed from synthetic seismic catalogues of stimulated reservoirs allow estimation of maximum hourly occurrence rates of induced seismic events for a given reservoir and fixed stimulation strategy. As opposed to the traditional probabilistic seismic hazard assessment approach (PSHA), this method is called forward induced seismic hazard assessment (FISHA).

Gischig and Wiemer (2013) used a 2D flow model with non-linear pore pressure diffusion in combination with a stochastic seed model. The transient pressure field was used to trigger seismicity at randomly distributed seed points. A differential stress normal distribution was assigned at each seed point, which is a potential seismic hypocentre. As in previous models, Mohr–Coulomb failure was assumed as well as an inverse relationship between stress drop and b-value (*Scholz*, 1968). Random seismic magnitudes were assigned from b-values corresponding to stress drop values at seed points. These are the main assumptions of *Gischig and Wiemer*
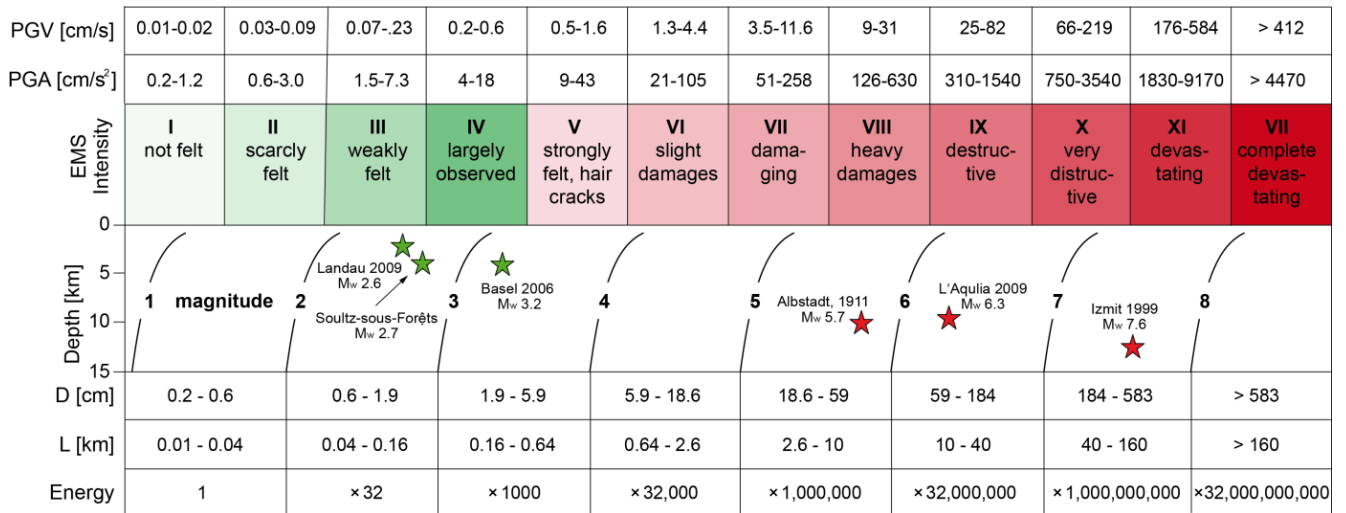
Figure 7. Earthquake fault scaling relationship. Rows indicate ground motion parameters, macro-seismic intensity (EMS) and earthquake moment magnitude in relation to fault properties (**D**, **L**) and energy of the rupture process. Selected EGS seismicity (green stars) and tectonic earthquakes (red stars) are shown in depth section. The boundary between intensity IV (dark green) and intensity V (light red) is indicated by a change in colour. (For interpretation of the references to colour in this figure legend, the reader is referred to the web version of the article.)

(2013), who generated synthetic seismic catalogues to reproduce the Basel induced seismicity data.

At this stage, we rely on the synthetic induced seismicity catalogues from *Yoon et al.* (2013, 2014) because their hydro-mechanically coupled model approach using dynamic fracture growth and interaction principles (Fig. 8) captures basic physical principles of the natural fracturing process operating in situ during the development of a geothermal field, and in addition reproduce main features of observed seismic catalogues monitored in EGS stimulation (post shut-in larger magnitude events, development of induced seismic cloud in the direction of maximum principal stress, magnitude-frequency distributions of events for different injection scenarios).

In the empirical approach (3), the size of the activated geothermal reservoir is determined by the extent of the hypocentre distribution of the induced events in hot-dry-rock projects – the so-called seismic cloud (*Fehler et al.*, 2001). In a critically stressed crust, however, the maximum possible event released during fluid injection into the reservoir cannot be captured with either a deterministic or empirical approach using the moment release – volumetric expansion hypothesis by *McGarr* (1976). Instead one needs to take into account crack interaction processes either by prescribed shear avalanche (*Baisch et al.*, 2010), or mixed-mode crack growth models (*Yoon et al.*, 2013), in order to account for larger, dynamic moment release than predicted by the fluid volume injected (seismic cloud) alone. In addition, in such critically stressed environments, the influence of remote triggering is much higher (*Jousset and Rohmer*, 2012). If no seismicity is observed, approaches (2) and (3) are inapplicable, and ambient seismic vibration studies need to be taken into account.

In summary, induced seismic hazard assessment should not rely on either deterministic or probabilistic methods alone. The hybrid approach by *Hakimhashemi et al.* (2013) combining deterministic, coupled hydromechanical reservoir models with forward induced seismic hazard assessment (FISHA) seems promising.

McGarr (2014) argued that maximum seismic moments, or moment magnitudes, for a given fluid injection activity can be estimated based on five plausible assumptions. (1) The formation is either seismogenic or there is hydraulic communication between the injection interval and seismogenic regions of the crust. The seismogenic regions, which are often Precambrian crystalline basement formations, contain numerous pre-existing faults, some of which are well oriented for failure in the ambient state of stress (e.g., *Townend and Zoback*, 2000). (2) Before injection, faults in the vicinity of the injection wells that are well oriented for slip in the ambient stress field are stressed to within a seismic stress drop of failure. (3) The rock mass is fully saturated before injection begins. (4) The seismic response to injection is a *Gutenberg and Richter* (1954) earthquake distribution $\log N = a - bM$, where M is moment-magnitude. (5) The induced earthquakes are localized to the region where the crust has been weakened due to fluid injection (*Hubbert and Rubey*, 1959). This last assumption seems plausible, but it is, nonetheless, difficult to prove that it always applies.

If these assumptions all apply, then it is straightforward to show that the maximum seismic moment and the maximum moment magnitude depend almost entirely on the total volume of fluid injected up to the time of the occurrence of the largest event (*McGarr*, 2014).

For most projects the maximum magnitude earthquake is observed to be much lower than estimated on the basis of injected fluid volume (see Fig. 1). For instance, the rock mass may respond to injection by deforming aseismically because of its material properties.

Table 3.

List of parameters, formulas and references used to compute earthquake fault scaling relationship shown in Fig. 7.

Parameter	Unit	Formula	Reference
Peak ground velocity, *PGV*	cm/s	$I_0 = 5.11 + 2.35 \log(PGV)$	*Faenza et al.* (2010)
Peak ground acceleration, *PGA*	cm/s²	$I_0 = 1.68 + 2.58 \log(PGA)$	
EMS Intensity, I_0		$M_w = 0.667\, I_0 + 0.30 \log(h) - 0.10$	*Grünthal et al.* (2009)
Displacement, *D*	cm	$\log(D) = 0.833 \log(L) - 1.07$	*Leonard* (2010)
Fault length, *L*	km	$M_w = 1.67\, \log(L) + 4.32$	

EMS, European Macroseismic Scale; M_w moment magnitude; I_0 epicentral intensity; h focal depth of earthquake.
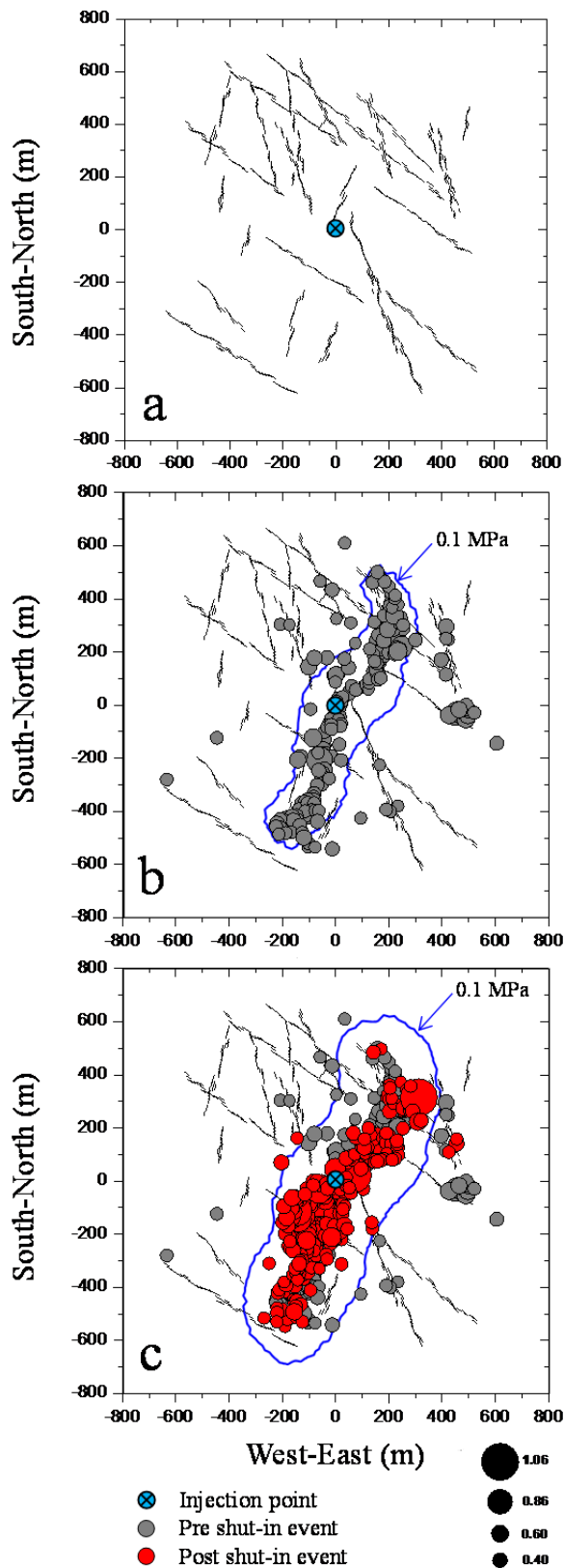
Figure 8. Discrete fracture network model with pore fluid flow algorithm (modified from *Yoon et al.*, 2014). (a) Naturally fractured reservoir with fluid injection point in the centre. (b) Stimulated reservoir with pre-shut-in induced seismic events (grey dots). (c) Post-shut-in events (red dots). In (b) and (c), the 0.1 MPa pore pressure contour is shown by blue solid line, and size of dots scales with seismic moment magnitude from mixed-mode dynamic fracture growth. The maximum horizontal stress is oriented in the North–South direction. (For interpretation of the references to color in this figure legend, the reader is referred to the web version of the article.)

5. Discussion

Baisch and Vörös (2010) compared seismic signatures of three crystalline geothermal reservoirs, Basel, Cooper Basin and Soultz-sous-Forêts. The deep seismicity at Soultz, whether viewed as a planar structure (*Charlety et al.*, 2007) or volumetric cloud (*Michelet and Töksöz*, 2007) is influenced by the existence of a larger tectonic fault in the Rhine Graben. This fault perturbs the in situ stress field with maximum horizontal stress striking N170°E (Table 1, *Cornet et al.*, 2007). Induced seismicity in the Cooper Basin reservoir is also associated with a larger fault and driven by the stress field (*Baisch et al.*, 2009). The stress regime in the Cooper Basin, however, is compressional, with maximum horizontal stress oriented E–W (Table 1). In this respect, induced seismicity at both sites is quite similar when accounting for the rotation of stresses (*Baisch and Vörös*, 2010). Since fractures propagate in the direction of maximum compressive stress, the seismic cloud at Soultz is oriented sub-vertical while the cloud in the Cooper Basin is oriented sub-horizontal. This relationship is shown schematically in Fig. 3 (inset, ellipses with arrows) for normal faulting (NF) and thrust faulting (TF) regime. Even if this is based on a simple fracture mechanics principle, Fig. 3 can serve as a first approach in estimating key parameters for the understanding of induced seismicity such as inflow, reservoir pressure and in situ stress. We rate in situ stress the second most important parameter in EGS development after the presence of heat. One should follow International Society for Rock Mechanics standards for determining in situ stress at a given (geothermal) site, *Stephansson and Zang* (2012).

Consistent with observations at Cooper Basin and Soultz, post-injection seismicity at Basel occurs at the outer boundary of the zone of previous seismic activity (*Häring et al.*, 2008). The field Kaiser Effect (*Baisch and Harjes*, 2003; absence of seismicity until the stress level of previous stimulations is exceeded) is a characteristic feature of geothermal sites located in hot granitic rock masses. In GEISER, this effect has also been documented in meta-greywacke at Berlin, El Salvador (*Kwiatek et al.*, 2014). In sedimentary basins, the Kaiser Effect has not been reported. The effect, however, has been discussed in the context of the collapse of a salt cavity (*Lebert et al.*, 2011).

In Fig. 9, two end-member cases of geothermal reservoir stimulation are shown, one for fluid injection into sedimentary rock (Fig. 9a and c), and one for injection into crystalline rock (Fig. 9b and d). The undisturbed rock under primary, in situ state of stress is shown in Fig. 9a and b. The future location of injection wells is shown by dashed circles. The perturbed stress state with borehole and fluid-stimulated rock mass (blue colour) is shown in Fig. 9c and d. In sedimentary rocks, isolated porosity (Fig. 9a and c, dots) can guide hydraulic fractures in the direction of maximum stress.

In the stimulation phase, mechanisms like pore collapse and grain crushing can lead to a more localized damage zone around the fluid-driven master tensile fracture (Fig. 9c). As a consequence, apart from mini-shear halos, the hydraulic fracture in sedimentary rock is dominated by implosion (pore collapse) and explosion sources (tensile cracks). In contrast, Fig. 9b and d illustrate the corresponding damage zone extension in hydraulic fracturing of crystalline rock. In Fig. 9b, the naturally fractured (saturated) crystalline host rock is shown before high pressure fluid injection. In Fig. 9d, the natural fracture network around the injection well allows for fast fluid transport into neighbouring fractures. Hydro-shear events along pre-existing, natural fractures in combination with tensile hydraulic opening at the very end of fractures (tips) may be the dominating mechanism in driving the overall hydraulic fracture in the direction of maximum stress. Branching of fractures is common if the energy required to generate new
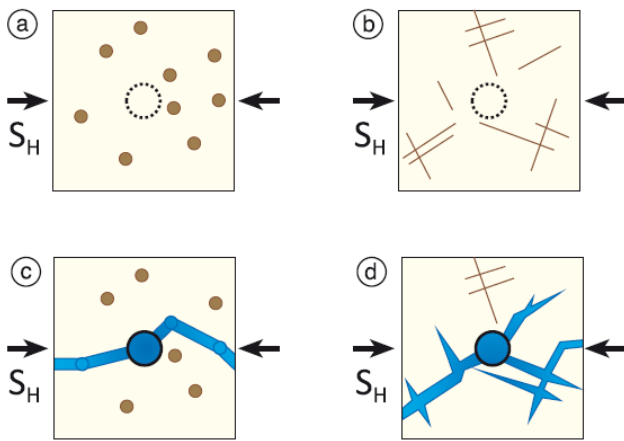
Figure 9. Synoptic picture of complex fracture modes in geothermal reservoirs. Sedimentary or weak volcanic rock (left) and crystalline rock (right) are displayed in an undisturbed stress state (upper panel, dashed circles indicate location of future borehole), and after fluid stimulation in a perturbed stress state (lower panel, with borehole). Horizontal section of reservoir at target depth is shown in an anisotropic stress field with fluid pathways (blue). (For interpretation of the references to colour in this figure legend, the reader is referred to the web version of the article.)

tensile fractures is lower or comparable to the energy required to reactivate existing, natural fractures. Depending on the initial fracture distribution around the well, the damage zone around the hydraulic fracture in crystalline rock may be much larger compared to the one in sedimentary rock. In the near field, however, injection into both rock types may suffer from the effect of an increasing number of tensile cracks due to elevated pore pressure discussed in Section 3.

Therefore, EGS development in weak volcanic rock (Fig. 9c and Table 1, e.g., Berlin El Salvador, Groß Schönebeck) may be quite different from permeability enhancement in crystalline rock (Fig. 9d and Table 1, e.g., Basel, Cooper Basin, Soultz-sous-Forêts). While in hard crystalline rock, dilatant shear may be the dominating mode II failure mechanism of the geothermal reservoir, in weak volcanic or sedimentary rock, subcritically stressed mode I fractures may chiefly be generated instead. This does not imply the absence of shear cracking in a sedimentary environment, but apart from accompanying propagating master-tensile fractures, dilatant shear may be of minor importance. This in turn can lead to a more persistent fracture growth path in sedimentary rock (Fig. 9c) where pores are interconnected by tensile crack growth. In contrast, in granitic reservoirs high-pressure fluid injection leads to a broader damage zone because the fluid can travel easily into pre-existing and newly-created fracture networks. Close to the stimulation well (near-field), tensile crack formation can dominate while in the far-field hydro-shears may predominate. The overall direction of fracture path in both rock types, however, is parallel to the maximum compressive stress (Fig. 9c and d). The width of the fracture damage zone is expected to be smaller for sedimentary than crystalline rock. If so, the seismic cloud in a sedimentary environment would be narrower because more localized damage in sedimentary rock produces less seismicity.

Based on this synoptic picture of complex fracture modes in geothermal reservoir stimulation, we recommend using high resolution source analyses of geothermal seismicity to determine what fracture mechanisms are operating in situ. Because the distribution of the seismic cloud in the reservoir strongly depends on the type and geometry of the seismic network, velocity model and location method used, its size cannot be related one-to-one to the actual fracture location

and mechanisms operating in situ, as evidenced by the difference in the extension of the acoustic (seismic) cloud and the actual fracture pattern observed in granite cores in the laboratory (*Zang et al.*, 2000). Although basic aspects of generating fluid-induced seismicity are understood, there are, nonetheless, gaps in our understanding of the key reservoir parameters that control the rate and magnitudes of the seismic events. All parameters may not be monitored, and triggering mechanisms may be of many different origins, including remote triggering (*Jousset and Rohmer*, 2012). Consequently, physics-based models are needed in a forward approach to analyse occurrence rate and maximum magnitude of induced seismic events in the development of a geothermal field.

Could seismogenic permeability (*Talwani et al.*, 2007) be the key to understanding the link between aseismic/relaxed and seismic/locked patches within the reservoir? Microseismicity results from a variety of causes. The spatiotemporal evolution of the triggering front depends on different parameters, including stress, injection rate, diffusivity and rock properties (e.g., friction coefficient). For example, an elliptical shape of the induced seismic cloud can be caused by the anisotropy of hydraulic diffusivity (*Shapiro et al.*, 1997, 1999), or by an anisotropic stress tensor (*Schoenball et al.*, 2010). Due to poroelastic effects, it is impossible to distinguish between the two types of anisotropy from geothermal seismicity alone. In addition, *Yoon et al.* (2014) using hydromechanical coupled discrete fracture network models demonstrated that also the injection scenario affects the shape of the seismic cloud. A clear understanding of the physical processes operating at the border between seismically inactive and seismically active zones (asperity, hydraulic barrier) needs to be developed. On a longer than stimulation perspective (production), processes like heat transport coupling and geochemical effects may dominate induced seismicity in hydrothermal systems.

6. Conclusions

Based on the analysis of seismicity associated with the development of geothermal sites compared to wastewater disposal and KTB ultra-deep fluid-injection experiments into the Earth's crust, a synoptic picture of the damage zone evolution in fluid-driven fractures during stimulation of enhanced geothermal systems (EGS) is developed and used to understand the relation between hydromechanical reservoir parameters (injectivity, fluid volume), the state of stress at depth, and the occurrence of larger magnitude seismic events (LME) in space and time during the stimulation phase of EGS sites. We draw ten conclusions.

(1) The maximum observed seismic magnitude increases with the volume of the fluid injected into the Earth's crust. Compared to waste water disposal wells, geothermal operations (in particular EGS stimulations) involve less fluid volume resulting in smaller maximum magnitudes. In crystalline reservoirs with multiple stimulation wells, seismicity is absent until the stress level of previous stimulations is exceeded (Kaiser Effect). Previous stimulations change the near-well stress field for subsequent stimulations. Stress mapping while injecting fluid is strongly recommended.

(2) A seismic network consisting of both, borehole and surface stations, allows increasing the network sensitivity towards lower event magnitudes and improves the magnitude of completeness. E.g. at the Basel EGS, the minimum magnitude and the magnitude of completeness of surface data were M_w 0.9 and 1.5, in contrast to M_w 0.1 and 0.8 for the borehole data. Including borehole data in the processing and interpretation of seismic lines im-

proves the depth resolution of the models. High quality of the velocity model is vital, because it determines the accuracy of hypocentre locations, source parameters and their temporal changes in EGS operations.

(3) Background seismicity should be monitored prior to any stimulation activity to obtain a baseline to evaluate changes in the seismicity rate during stimulation. In the absence of induced seismicity, ambient seismic vibrations can help in determining structural features and temporal changes in reservoir properties. Such data need to be acquired before the first stimulation, such that baseline data are available for comparison at a later stage.

(4) Local geological structures and seismic velocities should be mapped during the first stimulation phase of a geothermal reservoir. Fracture mapping is recommended down to the reservoir depth. In the stimulation phase, new fractures are created. Careful seismic monitoring is needed to maintain control of this permeability-enhancing process. Continuous monitoring of induced seismicity is required from the beginning of the stimulation experiment to detect runaway fracturing, also along buried faults.

(5) Due to the nature of EGS sites (engineered fracture networks), these systems are characterized by higher injection rates (up to 100 l/s) compared to most wastewater disposal wells (injection rate < 20 l/s). Reservoir injectivity (ratio of maximum inflow to maximum wellhead pressure) indicates low values ($I < 1.5$) for waste water disposal sites and values up to 6.3 at EGS sites where creation of new fractures is desired.

(6) During the EGS stimulation phase, larger magnitude events (LME) occur often after shut-in at greater distances from the injection well. The probability of a LME increases with injection volume, even though there are geologic differences. We differentiate between long-term injection operations (reservoir impoundment, waste water disposal) generating relatively larger LME compared to short-term fluid injection. Of the short-term injections, EGS stimulations have in general shown a higher propensity to produce LME, compared to hydraulic fracturing in oil and gas operations.

(7) Early during the stimulation phase and close to the injection well, pore pressures are generally high (near-field). In this situation, many small events are induced, often on faults with low applied shear stress, consistent with high b-values, low stress drops and significant volumetric components of the focal mechanisms. As the injected water migrates away from the injection point and the pore pressure decreases (far-field), the volumetric component of the focal mechanism becomes less significant and the shear stress necessary to trigger events increases. This is reflected in higher stress drops and in lower b-values. The latter implies a higher probability for the occurrence of LME at the periphery of the stimulated volume and during the later stages of the stimulation.

(8) Activities to optimize reservoir performance cause temporal changes of physical rock properties such as cooling of rock as well as dissolution and precipitation processes after long term circulation. Velocity ratios (Vp/Vs) are indicative of fluid path ways and pore-fluid aggregate in the fractured rock mass. For the analysis of seismicity and the local seismic velocity, 4D velocity tomography is needed. Since significant portions of aseismic slip cannot be ruled out at EGS sites, seismic monitoring should be conducted in concert with tilt metre measurements.

(9) EGS development in weak volcanic or sedimentary rocks (e.g., Berlin, El Salvador, Groß Schönebeck) may be very different from the permeability enhancement process in crystalline rocks (e.g., Basel, Cooper Basin, Soutz-sous-Forets). While in hard rock dilatant shear may be the dominating failure mechanism (mode II) in EGS stimulation, in sedimentary formations sub-critically stressed tensile cracks (mode I) may be chiefly generated instead. The width of the fluid-driven damage zone in naturally fractured crystalline rock is expected to be wider than that for sedimentary formations. If so, the seismic cloud induced by EGS stimulation should be narrower in weak compared to hard rocks (under the assumption of the same seismic resolution).

(10) Concerning seismic hazard potential at EGS sites, several approaches were discussed. In the structural geology approach, the maximum magnitude is inferred from the largest potentially active fault in the geothermal reservoir using an earthquake-fault relationship. Deterministic fracture model approaches use prescribed slip patches in slider spring models, or dynamic mixed-mode fracture models. Both models allow reproducing LME in the post shut-in phase of EGS stimulations. As opposed to the traditional, probabilistic seismic hazard assessment (PSHA) approach, we recommend to apply the hybrid technique FISHA (forward induced seismic hazard assessment) combining deterministic fracture models with probabilistic forward computations.

References

Ake, J., Mahrer, K., Connell, D.O., Block, L., 2005. Deep-injection and closely monitored induced seismicity at Paradox Valley, Colorado. Bull. Seismol. Soc. Am. 95, 664–683.

Albaric, J., Oye, V., Langet, N., Hasting, M., Lecomte, I., Messeiller, M., 2014. Monitoring of induced seismicity during the first geothermal reservoir stimulation at Paralana, Australia. Geothermics 52, 120–131.

Amitrano, D., 2003. Brittle–ductile transition and associated seismicity: experimental and numerical studies and relationship with the b value. J. Geophys. Res. 108 (B1), 2044, http://dx.doi.org/10.1029/2001JB000680.

Asanuma, H., Nozaki, H., Niitsuma, H., Wyborn, D., 2005. Interpretation of microseismic events with larger magnitude collected at Cooper Basin, Australia. Geotherm. Resour. Council Trans. 29, 87–91.

Bachmann, C., Wiemer, S., Goertz-Allmann, B., Woessner, J., 2012. Influence of pore pressure on the size distribution of induced earthquakes. Geophys. Res. Lett. 39, 9, http://dx.doi.org/10.1029/2012GL051480.

Baisch, S., Harjes, H.-P., 2003. A model for fluid-injection-induced seismicity at the KTB, Germany. Geophys. J. Int. 152, 160–170.

Baisch, S., Vörös, R., 2009. Induced seismicity, Technical Report SERIANEX, AP3000, Appendix 2., pp. 56–59.

Baisch, S., Vörös, R., 2010. Reservoir induced seismicity: where, when, why and how strong? In: Proceedings of World Geothermal Congress 2010, Bali, Indonesia, 25–29 April 2010.

Baisch, S., Weidler, R., Vörös, R., Wyborn, D., DeGraaf, L., 2006. Induced seismicity during stimulation of a geothermal HFR reservoir in the Cooper Basin (Australia). Bull. Seismol. Soc. Am. 96, 2242–2256.

Baisch, S., Vörös, R., Weidler, R., 2009. Investigation of fault mechanisms during geothermal reservoir stimulation experiments in Cooper Basin, Australia. Bull. Seismol. Soc. Am. 99 (1), 148–158.

Baisch, S., Vörös, R., Rothert, E., Stang, H., Jung, R., Schellschmidt, R.,

2010. A numerical model for fluid injection induced seismicity at Soultz-sous-Forêts. Int. J. Rock Mech. Mining Sci. 47, 405–413.

Bame, D., Fehler, M., 1986. Observations of long period earthquakes accompanying hydraulic fracturing. Geophys. Res. Lett. 13 (1), 149–152.

Batchelor, A.S., Garnish, J.D., 1990. The industrial exploitation of geothermal resources in Europe. Tectonophysics 178, 269–276.

Bommer, J.J., Oates, S.J., Cepeda, M., Lindholm, C., Bird, J., Torres, R., Marroquin, G., Rivas, J., 2006. Control of hazard due to seismicity induced by a hot fractured rock geothermal project. Eng. Geol. 83, 287–306.

Bromley, C.J., 2010. Promoting beneficial environmental effects and improving long-term utilization strategies through IEA-GIA collaboration. In: Proceedings of World Geothermal Congress 2010, Bali, Indonesia, 25–29 April 2010.

Bromley, C.J., Pearson, C.F., Rigor Jr., D.M., PNOC-EDC, 1986. Micro-earthquakes at the Puhagan geothermal field, Philippines – a case of induced seismicity. J. Volcanol. Geotherm. Res. 31 (3–4), 293–311.

Bruel, D., 2007. Using the migration of the induced seismicity as a constraint for fractured Hot Dry Rock reservoir modeling. Int. J. Rock Mech. Mining Sci. 44, 1106–1117.

Bruhn, D., Huenges, E., Ágústsson, K., Zang, A., Kwiatek, G., Rachez, X., Wiemer, S., van Wees, J.-D., Calcagno, P., Kohl, T., Dorbath, C., de Natale, G., Oye, V., 2011. Geothermal engineering integrating mitigation of induced seismicity in reservoirs – The European GEISER Project. Geotherm. Res. Council Trans. 35, 1623–1626.

Calcagno, P., Bouchot, V., Thinon, I., Bourgine, B., 2012. A new 3D fault model of the Bouillante geothermal province combining onshore and offshore structural knowledge (French West Indies). Tectonophysics 526–529, 185–195.

Calò, M., Dorbath, C., Cornet, F., Cuenot, N., 2011. Large scale aseismic motion identified through 4D P wave tomography. Geophys. J. Int. 186, 1295–1314.

Calò, M., Dorbath, C., Frogneux, M., 2014. Injection tests at the EGS reservoir of Soultz-sous-Forêts, Seismic response of the GPK4 stimulations. Geothermics 52, 50–58.

Castagna, J.P., Batzle, M.L., Eastwood, R.L., 1985. Relationships between compressional-wave and shear-wave velocities in clastic silicate rocks. Geophysics 50, 571–581.

Charlety, J., Cunot, N., Dorbath, L., Haessler, H., Frogneux, M., 2007. Large earthquakes during hydraulic stimulations at the geothermal site of Soultz-sous-Forêts. Int. J. Rock Mech. Mining Sci. 44, 1091–1105.

Clarke, D., Brenguier, F., Froger, J.-L., Shapiro, N.M., Peltier, A., Staudacher, T., 2013. Timing of a large volcanic flank movement at Piton de la Fournaise volcano using noise-based seismic monitoring and ground deformation measurements. Geophys. J. Int., http://dx.doi.org/10.1093/gji/ggt/276.

Cornet, F., Berard, T., Bourouis, S., 2007. How close to failure is a granitic rock mass at 5 km depth? Int. J. Rock Mech. Mining Sci. 44, 47–66.

Cuenot, N., Dorbath, C., Dorbath, L., 2008. Analysis of the microseismicity induced by fluid injections at the EGS site of Soultz-sous-Forêts (Alsace, France): implications for the characterization of the geothermal reservoir properties. Pure Appl. Geophys. 165, 707–828.

de Pater, C.J., Baisch, S., 2011. Geomechanical Study of Bowland Shale Seismicity. Cudrilla Resources Ltd, pp. 57, www.cuadrillaresources.com/wp-content/uploads/2012/02/Geomechanical-Study-of-Bowland-Shale-Seismicity_02-11-11.pdf

Deichmann, N., Ernst, J., 2009. Earthquake focal mechanisms of the induced seismicity in the 2006 and 2007 below Basel (Switzerland). Swiss J. Geosci. 102, 457–466.

Deichmann, N., Giardini, D., 2009. Earthquakes induced by the stimulation of enhanced geothermal system below Basel (Switzerland). Seismol. Res. Lett. 80, 784–798.

Deichmann, N., Kraft, T., Evans, K., 2014. Mapping of faults activated by the stimulation of the Basel enhanced geothermal system. Geothermics 52, 74–83.

Dorbath, L., Cuenot, N., Genter, A., Frogneux, M., 2009. Seismic response of the fractured and faulted granite to massive water injection at 5 km depth at Soultz-sous-Forêts (France). Geophys. J. Int., http://dx.doi.org/10.1111/j.1365-246X.2009.04030.x.

Dost, B., Haak, H.W., 2007. Natural and induced seismicity. In: Wong, Th0E., Batjes, D.A.J., de Jager, J. (Eds.), Geology of the Netherlands. Royal Netherlands Academy of Arts and Sciences, pp. 223–239.

Douglas, J., Jousset, P., 2011. Modeling the difference in ground-motion magnitude-scaling in small and large earthquakes. Seismic Res. Lett.

82, 504–508, http://dx.doi.org/10.1785/gssrl.82.4.504.

Dyer, B.C., Jones, R.H., Cowles, J.F., Barkved, O., Folstad, P.G., March 1999. Microseismic survey of a North Sea reservoir. World Oil, 74–78.

Economides, M.J., Saputelli, L., 2005. Chapter 6.2. Production optimization. In: Amadei, C. (Ed.), Encyclopedia of Hydrocarbons. Vol. 1 Exploration, Production and Transport. Fondata da Giovanni Treccani S.p.A, Rome, Italy, pp. 725–760.

Evans, L., Moriya, H., Niitsuma, H., Jones, R.H., Phillips, W.S., Genter, A., Sausse, J., Jung, R., Baria, R., 2005. Microseismicity and permeability enhancement of the hydrologic structures during massive fluid injections into granite at 3 km depth at Soultz HDR site. Geophys. J. Int. 160, 388–412.

Evans, K.F., Zappone, A., Kraft, T., Deichmann, N., Moia, F., 2012. A survey of the induced seismic responses to fluid injection in geothermal and CO 2 reservoirs in Europe. Geothermics 41, 30–54.

Faenza, L., Michelini, A., 2010. Regression analysis of MCS intensity and ground motion parameters in Italy and its application in ShakeMap. Geophys. J. Int. 180, 1138–1152.

Fehler, M., Jupe, A., Asanuma, H., 2001. More than cloud: new techniques for characterizing reservoir structure using induced seismicity. Lead. Edge 20, 324–328.

Ferrazzini, V., Chouet, B., Fehler, M., Aki, K., 1990. Quantitative analysis of long-period events recorded during hydrofracturing experiments at Fenton Hill, New Mexico. J. Geophys. Res. 95, 21871–21884.

Fischer, T., Hainzl, S., Eisner, L., Shapiro, S.A., Le Calvez, J., 2008. Microseismic signatures of hydraulic fracture growth in sediment formations: observations and modelling. J. Geophys. Res. 113, B02307, http://dx.doi.org/10.1029/2007JB005070.

Fix, J.E., Adair, R.G., Fisher, T., Mahrer, K., Mulcahy, C., Myers, B., Swanson, J., Woerpel, J.C., 1989. Development of Microseismic Methods to Determine Hydraulic Fracture Dimensions, Gas Technology Institute Technical Report No. 89-0116.

Frohlich, C., Hayward, C., Stump, B., Potter, E., 2011. The Dallas–Fort Worth earthquake sequence: October 2008 through May 2009. Bull. Seismol. Soc. Am. 101 (1), 327–340, http://dx.doi.org/10.1785/0120100131.

Frohlich, C., Ellsworth, W., Brown, W.A., Brunt, M., Luetgert, J., MacDonald, T., Walter, S., 2014. The 17 May 2012 M4.8 earthquake near Tipson, east Texas: an event possibly triggered by fluid-injection. J. Geophys. Res. Solid Earth 119, 581–593, http://dx.doi.org/10.1002/2013JB010755.

Giardini, D., 2009. Geothermal quake risk must be faced. Nature 426, 848–849.

Gischig, V.S., Wiemer, S., 2013. A stochastic model for induced seismicity based on non-linear enhancement. Geophys. J. Int., http://dx.doi.org/10.1093/gji/ggt164.

Goertz-Allmann, B.P., Goertz, A., Wiemer, S., 2011. Stress drop variations of induced earthquakes at the Basel geothermal site. Geophys. Res. Lett. 38, L09308, http://dx.doi.org/10.1029/ 2011GL047498.

Gritto, R., Jarpe, S.P., 2014. Temporal variations of VP/VS ratio at The Geysers geothermal field, USA. Geothermics 52, 112–119.

Grünthal, G., 2014. Induced seismicity related to geothermal projects versus natural tectonic earthquakes and other types of induced seismic events in Central Europe. Geothermics 52, 22–35.

Grünthal, G., Stromeyer, D., Wahlström, R., 2009. Harmonization check of Mw within the central, northern, and northwestern European earthquake catalogue (CENEC). J. Seismol. 13, 613–632.

Gupta, H.K., 2002. A review of recent studies of triggered earthquakes by artificial water reservoirs with special emphasis on earthquakes in Koyna, India. Earth Sci. Rev. 58 (3–4), 279–310.

Gupta, H.K., 2011. Artificial water reservoir triggered earthquakes. In: Gupta, H.K. (Ed.), Encyclopedia of Solid Earth Geophysics, vol. I. Springer Science and Business Media B.V., Dordrecht, The Netherlands, pp. 15–24.

Gutenberg, B., Richter, C., 1954. Seismicity in the Earth, 2nd ed. Princeton University Press, Princeton, NJ, pp. 16–25.

Hakimhashemi, A.H., Yoon, J.-S., Heidbach, O., Zang, A., Grünthal, G., 2013. FISHA – Forward induced seismic hazard assessment application to synthetic seismicity catalogue generated by hydraulic stimulation modeling. In: Proceedings of Thirty-Eight Workshop on Geothermal Reservoir Engineering Stanford University, Stanford, CA, STP-TR-198, pp. 455–461.

Hakimhashemi, A.H., Schoenball, M., Heidbach, O., Zang, A., Grünthal, G., 2014. Forward modelling of seismicity rate changes in georeservoirs with a hybrid geomechanical–statistical prototype model. Geothermics 52, 185–194.

Häring, M.O., Schanz, U., Ladner, F., Dyer, B.C., 2008. Characterization of Basel 1 enhanced geothermal system. Geothermics 37, 469–495.

Hasting, M., Albaric, J., Oye, V., Reid, R., Messeiller, M., Llanos, E., Malin, P., Shalev, E., Hogg, M., Alvarez, M., Miller, A., Walter, C., Boese, C., Voss, N., 2011. Real-time induced seismicity monitoring during wellbore stimulation at Paralana-2, South Australia. In: Australian Geothermal Energy Conference 2011.

Hazzard, J.F., Young, R.P., 2004. Dynamic modelling of induced seismicity. Int. J. Rock Mech. Mining Sci. 41, 1365–1376.

Healy, J.H., Rubey, W.W., Griggs, D.T., Raleigh, C.B., 1968. The Denver earthquakes. Science 161 (3848), 1301–1310.

Henderson, J.R., Barton, D.J., Foulger, G.R., 2002. Fractal clustering of induced seismicity in The Geysers geothermal area, California. Geophys. J. Int. 139 (2), 317–324. Herrmann, R.B., Park, S.-K., Wang, C.-Y., 1981. The Denver earthquakes of 1967–1968. Bull. Seismol. Soc. Am. 161, 1301–1310.

Holschneider, M., Zöller, G., Clements, R., Schorlemmer, D., 2014. Can we test for the maximum possible earthquake magnitude? J. Geophys. Res. Solid Earth 119, 2019–2028, http://dx.doi.org/10.1002/2013JB010319.

Horton, S., 2012. Disposal of hydrofracking waste fluid by injection into subsurface aquifers triggers earthquake swarm in central Arkansas with potential for damaging earthquake. Seismol. Res. Lett. 83, 250–260.

Hsieh, P.A., Bredehoft, J.D., 1981. A reservoir analysis of the Denver earthquakes: a case of induced seismicity. J. Geophys. Res. 86, 903–920.

Hubbert, K.M., Rubey, W.W., 1959. Role of fluid pressure in mechanics of overthrust faulting: parts I and II. Geol. Soc. Am. Bull. 70, 115–205.

Hubbert, K.M., Willis, D.G., 1957. Mechanics of hydraulic fracturing. Petrol. Trans. AIME T.P. 4597 210, 153–166.

Huenges, E., Trautwein, U., Legarth, B., Zimmermann, G., 2006. Fluid pressure variation in a sedimentary geothermal reservoir in the North German Basin: case study Groß-Schönebeck. Pure Appl. Geophys. 163, 2141–2152.

Hunt, T.M., Latter, J.H., 1982. A survey of seismic activity near Wairakei geothermal field, New Zealand. J. Volcanol. Geotherm. Res. 14 (3–4), 319–334.

Jost, M.L., Busselberg, T., Jost, O., Harjes, H.-P., 1998. Source parameters of injection-induced microearthquakes at 9 km depth at the KTB deep drilling site, Germany. Bull. Seismol. Soc. Am. 88, 815–832.

Jousset, P., Rohmer, J., 2012. Evidence for remotely triggered microearthquakes during salt cavern collapse. Geophys. J. Int. 191, 207–223, http://dx.doi.org/10.1111/j.1365-246X.2012.05598.x.

Jousset, P., Haberland, C., Bauer, K., Arnason, K., Weber, M., Fabriol, H., 2010. Seismic tomography and long-period earthquakes observation and modelling at the Hengill geothermal system. In: Proceedings World Geothermal Congress, Bali, Indonesia, 25–29 April 2010.

Jousset, P., Haberland, C., Bauer, K., Arnason, K., 2011. Hengill geothermal volcanic complex (Iceland) characterized by integrated geophysical observations. Geothermics 40, 1–24.

Jung, R., 2013. EGS–Goodbye of back to the future. In: Bunger, A.P., McLennon, J., Jeffrey, R. (Eds.), Earth Planetary Sciences, Geology and Geophysics, Effective and Sustainable Hydraulic Fracturing., http://dx.doi.org/10.5772/56458, ISBN 978-953-51-1137-5.

Keranen, K.M., Savage, H.M., Abers, G.A., Cochran, E.S., 2013. Potentially induced earthquakes in Oklahoma, USA: links between wastewater injection and the 2011 Mw 5.7 earthquake sequence. Geology, http://dx.doi.org/10.1130/G34045.1.

Kijko, A., 2004. Estimation of the maximum earthquake magnitude, Mmax. Pure Appl. Geophys. 161, 1655–1681.

Kim, W.-Y., 2013. Induced seismicity associated with fluid injection into a deep well in Youngstown, Ohio. J. Geophys. Res. Solid Earth 118, 3506–3518.

Kraft, T., Deichmann, N., 2014. High-precision relocation and focal mechanism of the injection induced seismicity at the Basel EGS. Geothermics 52, 59–73.

Kraft, T., Mai, P.M., Wiemer, S., Deichmann, N., Ripperger, J., Kästli, P., Bachmann, C., Fäh, D., Wössner, J., Giardini, D., 2009. Enhanced geothermal systems: mitigation risk in urban areas. EOS Trans. Am. Geophys. Union 90, 273–274.

Kwiatek, G., Bohnhoff, M., Dresen, G., Schulze, A., Schulte, T., Zimmermann, G., Huenges, E., 2010. Microseismicity induced during fluid-injection: a case study from the geothermal site at Groß Schönebeck, North German Basin. Acta Geophys. 58, 995–1020.

Kwiatek, G., Bulut, F., Bohnhoff, M., Dresen, G., 2014. High-resolution

analysis of seismicity induced at Berlin geothermal field, El Salvador. Geothermics 52, 98–111.

Lebert, F., Bernardie, S., Mainsant, G., 2011. Hydroacoustic monitoring of a salt cavity: an analysis of precursory events of the collapse. Nat. Hazards Earth Syst. Sci. 11, 2663–2675, http://dx.doi.org/10.5194/nhess-11-2663-2011.

Leonard, M., 2010. Earthquake fault scaling: self-consistent relating of rupture length, width, average displacement, and moment release. Bull. Seismol. Soc. Am. 100, 1971–1988.

Lockner, D., Byerlee, J.D., 1972. Hydrofracure in Weber sandstone at high confining pressure and differential stress. J. Geophys. Res. 82, 2018–2026.

Lockner, D., Byerlee, J.D., 1992. Fault growth and acoustic emissions in confined granite. Appl. Mech. Rev. 45 (3 (part 2)), S165–S173.

Majer, E.L., Baria, R., Stark, M., Oates, S., Bommer, J., Smith, B., Asanuma, H., 2007. Induced seismicity associated with enhanced geothermal systems. Geothermics 36, 185–222.

Majer, E.L., Queen, J., Daley, T., Long, R., 2008. Proceedings of Annual Meeting of Society of Exploration Geophysicists, Houston, TX.

Maxwell, S.C., Rutledge, J., Jones, R., Fehler, M., 2010. Petroleum reservoir characterization using downhole microseismic monitoring. Geophysics 75, http://dx.doi.org/10.1190/1.3477966, 75A129–75A137.

McGarr, A., 1976. Seismic moments and volume change. J. Geophys. Res. 81 (8), 1487–1494.

McGarr, A., 2014. Maximum magnitude earthquakes by induced fluid injection. J. Geophys. Res. Solid Earth, http://dx.doi.org/10.1002/2013JB010597.

McGuire, R.K., 2004. Seismic Hazard and Risk Analysis, vol. MNO-10. Earthquake Engineering Research Institute, Oakland, CA, USA, pp. 221.

Megies, T., Wassermann, J., 2014. Microseismicity observed at a non-pressure-stimulated geothermal power plant. Geothermics 52, 36–49.

Mendecki, A.J., 1997. Seismic Monitoring in Mines. Chapman and Hal, London, UK, pp. 280.

Meremonte, M.E., Lahr, J.C., Frankel, A.D., Dewey, J.W., Crone, A.J., Overturf, D.E., Carver, D.L., Bice, W.T., 2002. Investigation of an earthquake swarm near Trinidad, Colorado, August–October 2001, Open-File Report 02-0073, U.S. Geological Survey., pp. 32.

Michelet, S., Töksöz, M.N., 2007. Fracture mapping in the Soultz-sous-Forêts geothermal field using microearthquake locations. J. Geophys. Res. 112, B07315, http://dx.doi.org/10.1029/2006JB00.4442.

Mogi, K., 1962. Magnitude frequency relation for elastic shocks accompanying fractures of various materials and some related problems in earthquakes. Bull. Earthquake Res. Inst. 40, 831–853.

Mulyadi, 2010. Case study: hydraulic fracturing experiment in the Wayang Windu Geothermal field. In: Proceedings World Geothermal Congress, Bali, Indonesia, 25–29 April 2010.

Nagano, K., Moriya, H., Asanuma, H., Sato, M., Niitsuma, H., Kaieda, H., 1994. Down-hole acoustic emission measurement of hydraulic fracturing in Ogachi HDR model field. J. Geotherm. Res. Soc. Jpn. 16, 85–108 (in Japanese).

Nicholson, C., Wesson, R.L., 1990. Earthquake hazard associated with deep well injection: A report to the U.S. Environmental Protection Agency, U.S. Geological Survey Bulletin 1951. United States Governmental Printing Office, Washington, DC, pp. 74.

Oppenheimer, D.C., 1986. Extensional tectonics at The Geysers geothermal area, California. J. Geophys. Res. 91, 11463–11476.

Oye, V., Chavarria, J.A., Malin, P.E., 2004. Determining SAFOD area microearthquake locations solely with Pilot Hole seismic array data. Geophys. Res. Lett. 31, L12S10, http://dx.doi.org/10.1029/2003GL019403.

Oye, V., Gharti, H.N., Kühn, D., Braathen, A., 2010. Microseismic monitoring of fluid injection at the Longyearbyen CO2-Lab, Svalbard. In: Ritter, J., Oth, A. (Eds.), Cahiers du Centre Européen de Géodynamique et de Séismologie, Proceedings of the Workshop, "Induced Seismicity", November 15–17, 2010, Luxembourg, p. 141, ISBN 978-2-91989-709-4.

Pearson, C., 1981. The relationship between microseismicity and high pore pressures during hydraulic stimulation experiments in low permeability granitic rocks. J. Geophys. Res. 86, 7855–7864.

Pine, J.R., Batchelor, A.S., 1984. Downward migration of shearing in jointed rock during hydraulic injections. Int. J. Rock Mech. Mining Sci. Geomech. Abst. 21 (5), 249–263.

Rutqvist, J., Oldenburg, C.M., Dobson, P.F., 2010. Predicting the spatial extend of injection-induced zones of enhanced permeability at the Northwest Geysers EGS demonstration project. In: 44th US Rock

Mechanics Symposium and 5th U.S.-Canada Rock Mechanics Symposium, Salt Lake City, UT June 27–30. American Rock Mechanics Association, pp. 10–502.

Sanjuan, B., Jousset, P., Pajot, G., Debeglia, N., de Michele, M., Brach, M., Dupont, F., Braibant, G., Lasne, E., Duré, F., 2010. Monitoring of the Bouillante geothermal exploitation (Guadeloupe, French West Indies) and the impact on its immediate environment. In: Proc. World Geothermal Congress 2010, Bali, Indonesia, 25–29 April 2010.

Schoenball, M., Müller, T.M., Müller, B.I.R., Heidbach, O., 2010. Fluid-induced micro-seismicity in pre-stressed rock masses. Geophys. J. Int. 180, 813–819.

Scholz, C.H., 1968. The frequency–magnitude relation of microfracturing in rock and its relation to earthquakes. Bull. Seismol. Soc. Am. 58 (1), 399–415.

Scholz, C.H., 1990. The Mechanics of Earthquakes and Faulting. Cambridge University Press, Cambridge, UK, pp. 439.

Schorlemmer, D., Wiemer, S., Wyss, M., 2005. Variations in earthquake-size distribution across different stress regimes. Nature 437 (7058), 539–542.

Shapiro, S.A., Dinske, C., 2007. Violation of the Kaiser effect by hydraulic-fracturing-related microseismicity. J. Geophys. Eng. 4, 378–383.

Shapiro, S.A., Huenges, E., Borm, G., 1997. Estimating the crust permeability from fluid-injection-induced seismic emission at the KTB site. Geophys. J. Int. 131, F15–F18.

Shapiro, S.A., Audigane, P., Royer, J.-J., 1999. Large-scale permeability tensor of rocks from induced microseismicity. Geophys. J. Int. 137, 207–213.

Shapiro, S.A., Dinske, C., Kummerow, J., 2007. Probability of a given-magnitude earthquake induced by a fluid injection. Geophys. Res. Lett. 34 (L22314), http://dx.doi.org/10.1029/2007GL031615.

Shapiro, S.A., Dinske, C., Langenbruch, C., Wenzel, F., 2010. Seismogenic index and magnitude probability of earthquakes induced during reservoir stimulations. Lead. Edge March 2010, 304–309.

Silitonga, T.H., Siahaan, E.E., Suroso, 2005. A Poisson's ratio distribution from Wadati diagram as indicator of fracturing of Lahendong geothermal field, North Sulawesi, Indonesia, WGC 2005, Antalya, Turkey, 24–29 April.

Simiyu, S.M., 1999. Induced seismicity during interference tests at OW-719, Kenya. J. Geotherm. 28, 785–802.

Stephansson, O., Zang, A., 2012. ISRM suggested methods for rock stress estimation – Part 5: Establishing a model for the in-situ stress at a given site. Rock Mech. Rock Eng. 45, 955–969.

Suckale, J., 2009. Induced seismicity in hydrocarbon fields. Adv. Geophys. 51, 55–106.

Talwani, P., Acree, A., 1985. Pore pressure diffusion and the mechanism of reservoir induced seismicity. Pure Appl. Geophys. 122, 947–965.

Talwani, P., Chen, L., Gahalaut, K., 2007. Seismogenic permeability, ks. J. Geophys. Res. 112, B07309, http://dx.doi.org/10.1029/2006JB004665.

Terakawa, T., Miller, S.A., Deichmann, N., 2012. High fluid pressure and triggered earthquakes in the enhanced geothermal system in Basel, Switzerland. J. Geophys. Res. 117, B07305, http://dx.doi.org/10.1029/2011JB008980.

Tester, J.W., Anderson, B., Batchelor, A., Blackwell, D., DiPippo, R., Drake, E., Garnish, J., Livesay, B., Moore, M.C., Nichols, K., Petty, S., Toksoz, N., Veatch, R., Augustine, C., Baria, R., Murphy, E., Negraru, P., Richards, M., 2006. The Future of Geothermal Energy: Impact of Enhanced Geothermal Systems (EGS) on the United States in the 21st Century. Mass. Institute of Technology, Cambridge, MA, USA, pp. 209.

Townend, J., Zoback, M.D., 2000. How faulting keeps the crust strong. Geology 28, 399–402.

Trifu, C.I. (Ed.), 2002. The mechanism of induced seismicity. Pure and Applied Geophysics 159(1–3), Topical Issue. Birkhäuser, Basel, p. 617.

Trifu, C.I. (Ed.), 2010. Monitoring induced seismicity. Pure Applied Geophysics, Topical Issue. Birkhäuser, Basel.

Trubitt, T., Walker, A.B., Browitt, C.W.A., 1987. Perceptible hydrofracture seismic events caused by the Hot-Dry-Rock geothermal project in Cornwall. In: Global Seismology Report Number 339, British Geological Survey, Edinburgh, UK, p. 23.

van Eck, T., Goutbeek, F., Haak, H., Dost, B., 2006. Seismic hazard due to small-magnitude, shallow-source, induced earthquakes in The Netherlands. Eng. Geol. 87, 105–121.

van Eijis, R.M.H.E., Mulders, F.M.M., Nepveu, M., Kenter, C.J., Scheffers, B.C., 2006. Correlation between hydrocarbon reservoir properties and induced seismicity in the Netherlands. Eng. Geol. 84, 99–111.

van Wees, J.-D., Buijze, L., van Thienen-Visser, K., Nepveu, M., Wassing, B., Orlic, B., Fokker, P., 2014. Natural stress and fault controls in induced seismicity: what can we learn from gas depletion in The Netherlands? Geothermics 52, 206–219.

Wassing, B., Orlic, B., Fokker, P., Thienen-Visser, K., van Wees, J.-D., Buijze, L., 2014. Coupled continuum modelling of fracture reactivation and induced seismicity during enhanced geothermal operations. Geothermics 52, 153–164.

Wells, D.L., Coppersmith, K.J., 1994. New empirical relationships among magnitude, rupture length, rupture width, rupture area and surface displacement. Bull. Seismol. Soc. Am. 84, 974–1002.

Wyss, M., 1979. Estimating maximum expectable magnitude of earthquakes from fault dimensions. Geology 7, 336–340.

Yamabe, T.H., Hamza, V.M., 1996. Geothermal investigations in a area of induced seismic activity, Northern Sao Paulo State, Brasil. Tectonophysics 253, 209–225.

Yoon, J.-S., Zang, A., Stephansson, O., 2013. Simulation of multi-stage hydraulic fracturing and induced seismicity in naturally fractured reservoir using PFC2D. In: Zhu, Detournay, Hart, Nelson (Eds.), Continuum and Distinct Element Numerical Modeling in Geomechanics. Itasca International Inc., Minneapolis, ISBN 978-0-9767577-3-3, paper 06-02.

Yoon, J.-S., Zang, A., Stephansson, O., 2014. Numerical investigation on optimized stimulation of intact and naturally fractured deep geothermal reservoirs using hydro-mechanical coupled discrete particles joints model. Geothermics 52, 165–184.

Zang, A., Stephansson, O., 2010. Stress Field of the Earth's Crust. Springer Science + Business Media B.V., Dordrecht, pp. 322.

Zang, A., Wagner, F.C., Dresen, G., 1996. Acoustic emission, microstructure, and damage model of dry and wet sandstone stressed to failure. J. Geophys. Res. 101 (B8), 17507–17521.

Zang, A., Wagner, F.C., Stanchits, S., Janssen, C., Dresen, G., 2000. Fracture process zone in granite. J. Geophys. Res. 105 (B10), 23651–23661.

Zang, A., Yoon, J.-S., Stephansson, O., Heidbach, O., 2013. Fatigue hydraulic fracturing by cyclic reservoir treatment enhances permeability and reduces induced seismicity. Geophys. J. Int. 195, 1282–1287.

Zhao, P., Oye, V., Kühn, D., Cesca, S., 2014. Double-couple and moment tensor solutions of seismicity induced by hydraulic stimulation of the geothermal site in Basel, Switzerland. Geothermics 52, 74–83.

Zhu, X., Gibson, J., Ravindran, N., Zinno, R., Sixta, D., 1996. Seismic imaging of hydraulic fractures in Carthage tight sands: a pilot study. Lead. Edge 15, 218–224.

Zoback, M.D., Harjes, H.-P., 1997. Injection-induced earthquakes and crustal stress at 9 km depth at the KTB deep drilling site, Germany. J. Geophys. Res. 102 (B8), 18477–18491.